Oblique reflections of internal gravity wave beams

by

Hussain H. Karimi

B.S., University of California, San Diego (2010)

Submitted to the Department of Mechanical Engineering
in partial fulfillment of the requirements for the degree of

Masters of Science in Mechanical Engineering

at the

MASSACHUSETTS INSTITUTE OF TECHNOLOGY

June 2012

Author .....
Department of Mechanical Engineering
May 11, 2012

Certified by .....
Triantaphyllos R. Akylas
Professor of Mechanical Engineering
Thesis Supervisor

Accepted by .....
David E. Hardt
Chairman, Department Committee on Graduate Theses

Oblique reflections of internal gravity wave beams

by

Hussain H. Karimi

Submitted to the Department of Mechanical Engineering
on May 11, 2012, in partial fulfillment of the
requirements for the degree of
Masters of Science in Mechanical Engineering

Abstract

We study nonlinear effects in reflections of internal gravity wave beams in a continuously stratified liquid which are incident upon a uniform slope at an oblique angle. Wave motion in a stratified fluid medium is unique in the sense that the anisotropy of stratification directs energy transport in a manner specified by the frequency of the driving mechanism. Since there is no spatial variation along the direction of the flow field, plane waves are exact nonlinear solutions of the governing equations. In general, energy is carried in the form of a wave beam, which is a superposition of plane waves having parallel wavevectors.

However, beams incident upon a surface interact with the reflected beam in a locally confined region. Nonlinear interactions in the vicinity of the reflection site where the incident and reflected beams overlap act as a source for the generation of higher order harmonics. Employing small-amplitude expansions, we determine the directions of propagation and the strength of primary and second-harmonic reflected beams. The energy associated with the secondary beam during steady-state conditions is also computed.

We find that in-plane reflections produce the strongest nonlinear reflections and that larger spatial variations of the incident beam profile produce stronger secondary beams.

Thesis Supervisor: Triantaphyllos R. Akylas
Title: Professor of Mechanical Engineering

Acknowledgments

It has been a fulfilling opportunity to study under the tutelage of Professor Triantaphyllos R. Akylas. The entirety of this work is a manifestation of his profound thought, lucid explanations, vast knowledge, and nurturing tutorship. I am indebted to his patience and guidance, and eagerly look forward to continuing my ongoing apprenticeship under his supervision.

The entire support staff at MIT is to be recognized for the exemplary assistance provided to the typically overwhelmed graduate student.

It must be known that my initial spark of curiosity was first kindled during my undergraduate years at UC, San Diego through the excellent courses conducted by the Mechanical Engineering faculty. The enthusiasm with which they shared their knowledge brought me to reverence with regards to the powerful methods of engineering analysis. Amongst the faculty, I have had the pleasure of receiving personal encouragement from Prof. J. C. del Álamo, Prof. S. Sarkar, and Prof. V. Lubarda. I have further had the fortunate opportunity to attend lectures held by Prof. R. R. Bitmead, Prof. E. Jayson, Prof. H. Murakami, Prof. S. Nemat-Nasser, Prof. K. K. Nomura, and Prof. J. W. Rottman, as well as many others.

I am obligated to give my most sincere gratitude to authors whose names I have only read in their books. These texts have incited a passion within me which I did not believe could be imparted from written word, and its authors have captured my full esteem: John D. Anderson, Steven Chapra, Stephen H. Crandall, Ken A. Dill, David J. Griffiths, R. Haberman, Michael J. Moran, Albert J. Rosa, Roland E. Thomas, Howard N. Shapiro, and Frank M. White have been indispensable instructors in my education.

Finally, I extend my appreciation towards my family who have supported me throughout. From a young age, I was taught the rewards of perseverance, hard work, and sincerity.

This work was supported in part by the National Science Foundation under grants DMS-098122 and DMS-1107335.

Contents

List of Figures

List of Tables

Chapter 1

Introduction and review

1.1 Motivation

Internal gravity waves are unique to continuously stratified media, in which the anisotropy of the system leads to singular features of wave propagation of disturbances to hydrostatic equilibrium. Relevant to meteorology and oceanography, there is a desire to understand energy transport within the atmosphere and the ocean. Although not the dominant factor in energy transport, internal gravity waves are by no means negligible. In the atmosphere, internal gravity waves affect wind speeds by carrying momentum from the ground to higher altitudes [2]. In the ocean, they are partially responsible for the gradual vertical temperature gradients [6]. In this thesis, we focus on the relevance particular to oceanography; that is the fluid medium of interest is a liquid.

The anisotropy of the fluid medium, due to stratification in the direction of gravity, leads to a skewed direction of wave propagation first experimentally verified by Mowbray and Rarity [14] in which the disturbance from hydrostatic equilibrium is created by an oscillating cylinder. In an isotropic medium, such a disturbing source would lead to cylindrical wavefronts; however, the vertical anisotropy here results in the pattern of wave propagation taking the form of four straight arms radiating away from the source. This cross pattern is known as St. Andrew's Cross (see figure 1-2).

A common mechanism of internal wave generation in the ocean is oscillating tidal

flow over underwater topography, such as ridges [4]. By the vertical component of energy transport, it is suggested that deep-sea mixing is influenced by internal wave generation and subsequent propagation [22]. The overall effect is believed to be partly responsible for the gradual temperature variation in the ocean [5].

Following the propagation of an internal wave, it is expected to observe its eventual interaction with topography redirecting energy transport leading to a modification of energy allocation. Phillips [16] first investigated the linear response of a plane wave incident upon a uniform slope, concluding that the reflected wave maintains the frequency of oscillation of the incident wave. Thorpe [21] then calculated higher-order nonlinear corrections before Tabaei et al. [19] further extended the solution to the more general case of nonlinear wave beams, which soon afterwards received qualitative, experimental verification [15]. Here, we attempt to broaden our understanding of reflections by allowing for an oblique angle to exist between the incident beam and the uniform slope.

This thesis is organized as follows. Chapter 1 first presents a brief review of some well-known, singular properties of internal gravity waves [6, 10, 13, 17]. Although the treatment in chapter 1 is easily found elsewhere, it is the author's hope that this chapter will inform the reader of the most pertinent concepts assumed throughout this work. Before beginning a detailed analysis of oblique reflections, chapter 2 opens with a discussion to motivate the plausible invocation of a weakly nonlinear model. Many of the details of this analysis have been included in hopes to aid the uninitiated into the exciting use of a myriad of mathematical techniques in action. Based on this theoretical analysis, we will then consider some sample computations in chapter 3, and finally close this thesis with a brief concluding discussion in chapter 4.

1.2 Brunt-Väisälä frequency

It is perhaps instructive to first consider the simplest sort of perturbation to a stably stratified fluid under the conditions of hydrostatic equilibrium. A fluid parcel vertically displaced is acted upon by the restoring buoyancy force which causes the

fluid parcel to accelerate towards its equilibrium position, but the ensuing gain in momentum results in its overshoot. Still displaced from equilibrium, the restoring force now acts in the opposite direction in an effort to restore the fluid parcel to its stable position. This oscillatory motion is much like a simple mass supported by a spring, which servers as the restoring force. Let us examine the details of this fluid motion as a starting point.

In a stratified fluid under hydrostatic equilibrium, the pressure $\overline{p}(z)$ and density $\overline{\rho}(z)$ satisfy

$$\frac{d\overline{p}}{dz} = -g\overline{\rho}, \tag{1.1}$$

where z denotes the vertical coordinate, measured upwards. Applying momentum principles to a differential fluid parcel that is initially located at z_0 and subsequently displaced by a short vertical distance δ, as shown in figure 1-1, we find in the vertical

$$(\overline{\rho}(z_0)\mathrm{d}V)\,\ddot{\delta} = \left[\overline{p}\left(z_0+\delta-\frac{1}{2}\mathrm{d}z\right) - \overline{p}\left(z_0+\delta+\frac{1}{2}\mathrm{d}z\right)\right]\mathrm{d}A - g\overline{\rho}(z_0)\mathrm{d}V. \tag{1.2}$$

Expanding the pressure terms around the displaced position, $z_0+\delta$, and dividing through by the parcel volume $\mathrm{d}V$,

$$\begin{aligned}\overline{\rho}(z_0)\ddot{\delta} &= \left[\frac{\left(-\frac{1}{2}\mathrm{d}z\right)\frac{d\overline{p}}{dz}(z_0+\delta) - \left(\frac{1}{2}\mathrm{d}z\right)\frac{d\overline{p}}{dz}(z_0+\delta)}{\mathrm{d}z}\right] - g\overline{\rho}(z_0)\\ &= -\frac{d\overline{p}}{dz}(z_0+\delta) - g\overline{\rho}(z_0).\end{aligned} \tag{1.3}$$

The hydrostatic pressure gradient is the buoyancy force and can be expressed in terms of the density stratification by the hydrostatic equilibrium (1.1) as

$$\frac{d\overline{p}}{dz}(z_0+\delta) = -g\overline{\rho}(z_o+\delta). \tag{1.4}$$

Now we expand about z_0 and substitute $\overline{\rho}(z_0+\delta) \approx \overline{\rho}(z_0) + \delta d\overline{\rho}(z_0)/dz$ into the momentum equation to find the equation of motion for simple vertical oscillations to

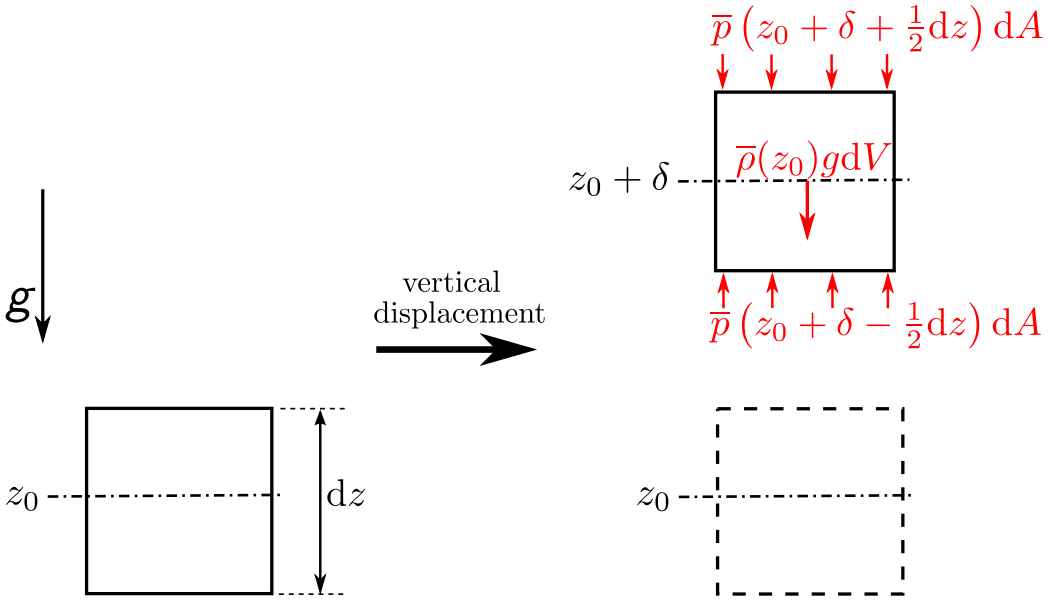

Figure 1-1: Fluid displaced from hydrostatic equilibrium. A fluid parcel initially at z_0 in its equilibrium position having density $\overline{\rho}(z_0)$, as shown on the left, is vertically displaced as shown on the right. The vertical forces in red are the surface pressure forces and the body weight of the parcel. A force balance reveals that the displaced fluid parcel oscillates vertically, much like a mass on a spring, with a frequency dependent on the strength of the local density stratification.

be

$$\overline{\rho}(z_0)\ddot{\delta} = g\frac{d\overline{\rho}}{dz}(z_0)\delta. \tag{1.5}$$

Since z_0 is arbitrary, that is for any fluid parcel vertically perturbed from its equilibrium position, the preceding equation is valid for any position z and we drop the point of evaluation z_0. Quite often, the equation of motion is written as

$$\ddot{\delta} + N^2\delta = 0, \tag{1.6}$$

where

$$N^2 \equiv -\frac{g}{\overline{\rho}}\frac{d\overline{\rho}}{dz} \tag{1.7}$$

is known as the *Brunt-Väisälä* frequency, or sometimes simply as the buoyancy frequency. It is a measure of the *local* density stratification and is useful in characterizing ocean (and atmospheric) flows. For a stably stratified fluid, density decreases in the direction opposing gravity so $d\overline{\rho}/dz < 0$ and $N^2 > 0$. Typical values of N are

$\sim 10^{-2}$ s^{-1} in the ocean and atmosphere [17]. The corresponding period of oscillation is on the order of 10 minutes.

1.3 Boussinesq approximation

To begin our model of internal wave propagation in the ocean, we first consider viscous effects in a post-priori fashion. Knowing beforehand that viscous effects scale as $1/\mathrm{Re}$, where $\mathrm{Re} \equiv \nu/UL$ is the Reynolds number, an estimate of the importance of viscous dissipation can be made by considering field observations. The kinematic viscosity of water is $\nu \sim 10^{-6}$ m^2/s and characteristic length and velocity scales are $L \sim 10$ m and $U \sim 1$ m/s, respectively. In turn, $1/\mathrm{Re} \sim 10^{-7}$ and it is clear that we can neglect viscous effects in many cases [17]. From here on, we will assume inviscid flow.

There are various ways to present a reasonable approximation to determine the flow due to perturbations from hydrostatic equilibrium in a stratified fluid [10, 17], each of which instructively leads to the same result known as the Boussinesq approximation. However, the reasoning provided between various sources is slightly different, though the essence is the same. Here, we will provide the details of the approximation as given by Tabaei and Akylas [18] since we believe that the application of the approximation in this fashion is done so in a manner which picks up all the subtleties and limitations in a single step. There is also the added advantage of removing the explicit presence of the hydrostatic density variation from the inviscid momentum equations. The mathematical reward of this simplification will be noted at the end of this section when it becomes apparent.

First, let us agree on the relevant equations and begin with inviscid momentum balance,

$$\varrho \frac{D\boldsymbol{u}}{Dt} = -\boldsymbol{\nabla} P - \varrho g \hat{\boldsymbol{e}}_z, \tag{1.8}$$

where $D/Dt \equiv \partial/\partial t + \boldsymbol{u} \cdot \boldsymbol{\nabla}$ is the material derivative following a fluid parcel, $\boldsymbol{u} = u\hat{\boldsymbol{e}}_x + v\hat{\boldsymbol{e}}_y + w\hat{\boldsymbol{e}}_z$ is the vector velocity field, $\hat{\boldsymbol{e}}_z$ is the unit vector oriented in the positive vertical direction, P is the total pressure, and ϱ is the total density. It will prove useful to invoke the constitutive relation appropriate to oceanography before

conserving mass. That is, the incompressibility condition such that any particular fluid parcel retains its density, ϱ, throughout the entirety of the flow, is stated as

$$\frac{D\varrho}{Dt} = 0. \tag{1.9}$$

Now substituting (1.9) into mass conservation

$$\boldsymbol{\nabla} \cdot \boldsymbol{u} = -\frac{1}{\varrho}\frac{D\varrho}{Dt},$$

we find that the right-hand side becomes identically zero, and the continuity equation,

$$\boldsymbol{\nabla} \cdot \boldsymbol{u} = 0, \tag{1.10}$$

requires the divergence of the flow field to be zero.

The appropriate scaling parameters are the typical wavelength L of an internal wave as length scale, $1/N_0$ as time scale where N_0 is a typical value of the Brunt-Väisälä frequency, and $\overline{\rho_0}$ a nominal value of density. The relative length scale of density variation $\mathcal{L}$ is also important and from (1.7) we find that it scales like

$$\mathcal{L} \sim g/N_0^2. \tag{1.11}$$

The Boussinesq parameter is the ratio of the two relevant length scales, $B \equiv L/\mathcal{L}$, so

$$B = LN_0^2/g. \tag{1.12}$$

To show that density perturbations scale like B, consider again the momentum equations (1.8), but with the substitution $\varrho = \overline{\rho} + \rho$ and $P = \overline{p} + p$ so that the hydrostatic variation (1.1) cancels out,

$$\varrho\frac{D\boldsymbol{u}}{Dt} = -\boldsymbol{\nabla}p - \rho g\hat{\boldsymbol{e}}_z. \tag{1.13}$$

In gravity waves we expect the the inertial terms to balance with buoyancy pertur-

bations, $\overline{\rho}\frac{Dw}{Dt} \sim \rho g$. Along with the parameters above, then, density perturbations,

$$\rho \sim \left(\frac{N_0^2 L}{g}\right)\overline{\rho_0} = B\overline{\rho_0}. \tag{1.14}$$

The result (1.14) anticipates the known result [10, 17].

To write the governing equations in the most convenient form for the ensuing analysis,

$$\varrho(\boldsymbol{x},t) = \overline{\rho}(z) + B\frac{\overline{\rho}(z)}{\overline{\rho_0}}\rho(\boldsymbol{x},t), \tag{1.15a}$$

$$P(\boldsymbol{x},t) = \overline{p}(z) + \frac{\overline{\rho}(z)}{\overline{\rho_0}}p(\boldsymbol{x},t). \tag{1.15b}$$

Note that the perturbations ρ and p are not simply the variations to hydrostatic equilibrium since these quantities are scaled with local hydrostatic density; instead, this locally scaled variable will allow the complete removal of the explicit presence of the hydrostatic density, $\overline{\rho}(z)$, within the Boussinesq approximation, from (1.8).

To see this, we first introduce (1.15) into (1.8),

$$\overline{\rho}\left(1 + B\frac{\rho}{\overline{\rho_0}}\right)\frac{D\boldsymbol{u}}{Dt} = -\boldsymbol{\nabla}\left(\overline{p} + \frac{\overline{\rho}}{\overline{\rho_0}}p\right) - g\overline{\rho}\left(1 + B\frac{\rho}{\overline{\rho_0}}\right)\hat{\boldsymbol{e}}_z. \tag{1.16}$$

The hydrostatic equilibrium terms drop by (1.1), and after dividing through by $\overline{\rho}$,

$$\left(1 + B\frac{\rho}{\overline{\rho_0}}\right)\frac{D\boldsymbol{u}}{Dt} = \frac{-\boldsymbol{\nabla}(\overline{\rho}p)}{\overline{\rho_0}\,\overline{\rho}} - gB\frac{\rho}{\overline{\rho_0}}\hat{\boldsymbol{e}}_z. \tag{1.17}$$

Distributing the gradient operator in the first term on the right-hand side and incorporating (1.7),

$$\frac{-\boldsymbol{\nabla}(\overline{\rho}p)}{\overline{\rho_0}\,\overline{\rho}} = -\frac{\boldsymbol{\nabla}p}{\overline{\rho_0}} - \frac{p(d\overline{\rho}/dz)}{\overline{\rho_0}\,\overline{\rho}}\hat{\boldsymbol{e}}_z = -\frac{\boldsymbol{\nabla}p}{\overline{\rho_0}} + \frac{N^2}{\overline{\rho_0}g}p\hat{\boldsymbol{e}}_z, \tag{1.18}$$

the momentum equation yields

$$\left(1 + B\frac{\rho}{\overline{\rho_0}}\right)\frac{D\boldsymbol{u}}{Dt} = -\frac{\boldsymbol{\nabla}p}{\overline{\rho_0}} - \left(gB\frac{\rho}{\overline{\rho_0}} - \frac{N^2}{\overline{\rho_0}g}p\right)\hat{\boldsymbol{e}}_z. \tag{1.19}$$

Similarly, (1.15) applied to the incompressibility condition (1.9),

$$\left(\frac{\partial}{\partial t} + \boldsymbol{u}\cdot\boldsymbol{\nabla}\right)\left[\overline{\rho}(z)\left(1 + B\frac{\rho}{\overline{\rho_0}}\right)\right] = 0. \tag{1.20}$$

Separating the local and advective derivatives, we distribute the latter per the product rule,

$$\left(B\frac{\overline{\rho}}{\overline{\rho_0}}\right)\frac{\partial\rho}{\partial t} + \left(B\frac{\overline{\rho}}{\overline{\rho_0}}\right)(\boldsymbol{u}\cdot\boldsymbol{\nabla})\,\rho + \left(1 + \frac{\rho}{\overline{\rho_0}}\right)w\frac{d\overline{\rho}}{dz} = 0. \tag{1.21}$$

Dividing through by $B\overline{\rho}/\overline{\rho_0}$, the factor in the third term can be simplified with the use of (1.7) and (1.12) as

$$\frac{\overline{\rho_0}}{B}\left(\frac{d\overline{\rho}/dz}{\overline{\rho}}\right) = -\frac{N^2\overline{\rho_0}}{(Bg)} = -\frac{N^2\overline{\rho_0}}{N_0^2 L}. \tag{1.22}$$

The incompressibility equation can then be written as

$$\left(\frac{\partial}{\partial t} + \boldsymbol{u}\cdot\boldsymbol{\nabla}\right)\rho - \frac{N^2\overline{\rho}_0}{N_0^2 L}\left(1 + B\frac{\rho}{\overline{\rho_0}}\right)w = 0. \tag{1.23}$$

Thus far, everything is exact. To make an order of magnitude approximation, the governing equations (1.10), (1.19) and (1.23), must first be appropriately nondimensionalized. The scaling parameters are reiterated in table 1.1 along with a list of the nondimensional variables which are specifically scaled so that they are all of the same order. The governing equations then become

$$(1 + B\rho)\left(\frac{\partial}{\partial t} + \boldsymbol{u}\cdot\boldsymbol{\nabla}\right)\boldsymbol{u} = -\boldsymbol{\nabla}p - \left(\rho - BN^2 p\right)\hat{\boldsymbol{e}}_z, \tag{1.24a}$$

$$\boldsymbol{\nabla}\cdot\boldsymbol{u} = 0, \tag{1.24b}$$

$$\left(\frac{\partial}{\partial t} + \boldsymbol{u}\cdot\boldsymbol{\nabla}\right)\rho - N^2(1 + B\rho)w = 0. \tag{1.24c}$$

All the field variables are $\mathcal{O}(1)$, which leaves the relative magnitude of different terms solely dependent on B. Furthermore, the Brunt-Väisälä frequency defined by (1.7) is nondimensionalized to

$$\frac{d\overline{\rho}}{dz} = -B\overline{\rho}N^2. \tag{1.25}$$

Scaling parameters			Nondimensional quantities		
dimension	based on	quantity			
length	typical wavelength	L	$\boldsymbol{u}/N_0 L$	$\rightarrow$	$\boldsymbol{u}$
time	typical Brunt-Väisälä frequency	N_0^{-1}	$\rho/\overline{\rho_0}$	$\rightarrow$	ρ
density	nominal density	$\overline{\rho_0}$	$P/N_0^2 L^2 \overline{\rho_0}$	$\rightarrow$	P
			N/N_0	$\rightarrow$	N

Table 1.1: The scaling parameters on the left-hand side are chosen so that they are appropriate to the wave motion of internal gravity waves. Applied to the field variables of interest, and to the buoyancy frequency N, we can easily compare the relative importance of the different terms in the governing equations simply by inspection. This method allows us to make clean approximations and clearly judge the limitations of them in doing so.

In one fell swoop, we now make the approximation that $B \to 0$, which is to say that the length scale associated with wave motion is much less than the length scale of relevant hydrostatic density variations. Inherent to this approximation then, is that $\overline{\rho} \to 1$ by (1.25). This means that a fluid parcel undergoing wave motion will experience spatial variations in which the local density is different, *however* those changes are considered to be quite small. Note that the entirety of the Boussinesq approximation is contained in $B \to 0$. The mathematical reward with our particular form of hydrostatic perturbations (1.15) mentioned earlier is that the momentum equations have constant coefficients, regardless of the background stratification, $\overline{\rho}$. We will further simplify the fluid system by considering the background stratification to be uniform ($N = 1$) so that (1.24) becomes

$$\left(\frac{\partial}{\partial t} + \boldsymbol{u} \cdot \boldsymbol{\nabla}\right) \boldsymbol{u} = -\boldsymbol{\nabla} p - \rho \hat{\boldsymbol{e}}_z, \tag{1.26a}$$

$$\boldsymbol{\nabla} \cdot \boldsymbol{u} = 0, \tag{1.26b}$$

$$\left(\frac{\partial}{\partial t} + \boldsymbol{u} \cdot \boldsymbol{\nabla}\right) \rho = w. \tag{1.26c}$$

Recall that we are taking the fluid to be incompressible from its hydrostatic equilibrium. That is, if we follow two different fluid parcels located at z_1 and z_2 during equilibrium conditions, they will have a density $\overline{\rho}(z_1)$ and $\overline{\rho}(z_2)$, respectively, for all time even when perturbed.

1.4 Internal gravity waves

The purpose of this chapter is to illustrate the physics of internal gravity waves, and for instructive purposes, we will take the total pressure and density to be $P = \overline{p} + p$ and $\varrho = \overline{\rho} + \rho$, respectively, in the governing (dimensional) equations (1.8), (1.9), and (1.10). For the remainder of this review chapter, we will work in the these terms to avoid confusion by calculating quantities which have very clear, unambiguous interpretations so that the basics of internal gravity are openly understood. We will return to the nondimensional equations (1.26) in chapter 2 where it will prove useful as it has in previous works [18, 19].

The Boussinesq approximation, in these dimensional terms, can then be applied to a uniform background stratification to reveal the equations of wave motion [10, 17]

$$\rho_0 \left(\frac{\partial}{\partial t} + \boldsymbol{u} \cdot \boldsymbol{\nabla} \right) \boldsymbol{u} = -\boldsymbol{\nabla} p - \rho g \hat{\boldsymbol{e}}_z, \tag{1.27a}$$

$$\boldsymbol{\nabla} \cdot \boldsymbol{u} = 0, \tag{1.27b}$$

$$\left(\frac{\partial}{\partial t} + \boldsymbol{u} \cdot \boldsymbol{\nabla} \right) \rho = -w \frac{d\overline{\rho}}{dz}. \tag{1.27c}$$

It is useful to first derive the linear solution which assumes small-amplitude waves and allows the neglect of the advective terms in (1.27),

$$\rho_0 \boldsymbol{u}_t = -\boldsymbol{\nabla} p - \rho g \hat{\boldsymbol{e}}_z, \tag{1.28a}$$

$$u_x + v_y + w_z = 0, \tag{1.28b}$$

$$\rho_t = -w \overline{\rho}_z, \tag{1.28c}$$

where (x, y, z, t)-subscripts denote derivatives. There are five unknowns with the same number of equations in the set (1.28). First, pressure is eliminated by taking the curl of the momentum equations [$\boldsymbol{\nabla} \times$(1.28a)] which yields,

$$\rho_0 (w_y - v_z)_t = -\rho_y g. \tag{1.29a}$$

$$\rho_0(w_x - u_z)_t = -\rho_x g. \tag{1.29b}$$

$$u_{ty} = v_{tx}. \tag{1.29c}$$

Note that (1.29) contains only two linearly independent equations, not three. By taking cross derivatives of (1.29a) and (1.29b), followed by the difference, we can re-construct (1.29c). This is expected since the elimination of a variable is associated with the usage of an equation.

Although it is possible to solve for any of the four remaining variables, it is most convenient to favour w. We will do so here by focusing on (1.29a) and allow our next steps be guided by the elimination of v followed by u. After taking the z-derivative of (1.28b), v is expressed as

$$-v_{yz} = u_{xy} + w_{zz}. \tag{1.30}$$

The result (1.30) can be substituted into the y-derivative of (1.29a),

$$\rho_0 \left(w_{yy} + u_{xz} + w_{zz}\right)_t = -\rho_{yy} g \tag{1.31}$$

The velocity component u is the next target of elimination and prepared for dispatch by considering the x-derivative of (1.29b),

$$\rho_0 u_{zxt} = \rho_0 w_{xxt} + \rho_{xx} g. \tag{1.32}$$

Substitution of (1.32) into (1.31) gives

$$\rho_0(w_{xx} + w_{yy} + w_{zz})_t = -g(\rho_{xx} + \rho_{yy}) \tag{1.33}$$

The last variable to go is density, leaving w isolated. Before invoking (1.28c), it must have its second x- and y- derivatives taken so to be matched with the t-derivative of the right-hand side of (1.33),

$$\rho_0(w_{xx} + w_{yy} + w_{zz})_{tt} = -g(\rho_{txx} + \rho_{tyy})$$

$$= g\overline{\rho}_z(w_{xx} + w_{yy}). \tag{1.34}$$

Rearranging, the linear solution represented in favour of the vertical velocity component is

$$\left\{ \frac{\partial^2}{\partial t^2} \nabla^2 + N^2 \nabla_{\mathrm{H}}^2 \right\} w = 0. \tag{1.35}$$

where $\nabla_{\mathrm{H}}^2 \equiv \partial^2/\partial x^2 + \partial^2/\partial y^2$ is the horizontal Laplacian operator and $N \equiv \sqrt{-\frac{g}{\rho_0}\frac{d\overline{\rho}}{dz}}$ is the Brunt-Väisälä frequency as before in §1.2.

Assuming a plane wave solution of the form

$$w = w_0 \exp\left\{ \mathrm{i}\left(\boldsymbol{k} \cdot \boldsymbol{x} - \omega t \right) \right\} = w_0 \exp\left\{ \mathrm{i}\left(kx + ly + mz - \omega t \right) \right\},$$

the dispersion relation is found from (1.35) as

$$\omega^2 = N^2 \frac{k^2 + l^2}{k^2 + l^2 + m^2} = N^2 \sin^2 \beta, \tag{1.36}$$

where β is the angle of the wavevector, $\boldsymbol{k}$, from the vertical, or equivalently the angle of propagation from the horizontal as shown in figure 1-2. For simplicity, we will take $l = 0$ by rotating our coordinate system by a horizontal angle of $\tan\phi = l/k$ so that the waves are now uniform in the new y-coordinate and the y-velocity component is $v = 0$. Because the system is horizontally isotropic, there is no loss by making this rotation.

The ambiguity associated with the signs of β and ω in (1.36) can be addressed in different ways, each requiring careful interpretation of the physics involved. Here, we will always consider $\omega > 0$. Furthermore, β will be taken from the vertical to the wavevector such that $\beta < \pi/2$ ($\sin\beta > 0$). In this way, β and ω are uniquely defined by (1.36) and can be written, according to our convention, as $\omega = N \sin\beta$.

To understand this particular geometry more clearly, we first calculate the phase velocity $\boldsymbol{c}$ and group velocity $\boldsymbol{c}_g$,

$$\boldsymbol{c} \equiv \frac{\omega}{|\boldsymbol{k}|}\hat{\boldsymbol{e}}_k = N \frac{k}{|\boldsymbol{k}|^3} \left\{ k\hat{\boldsymbol{e}}_x + m\hat{\boldsymbol{e}}_z \right\}, \tag{1.37a}$$

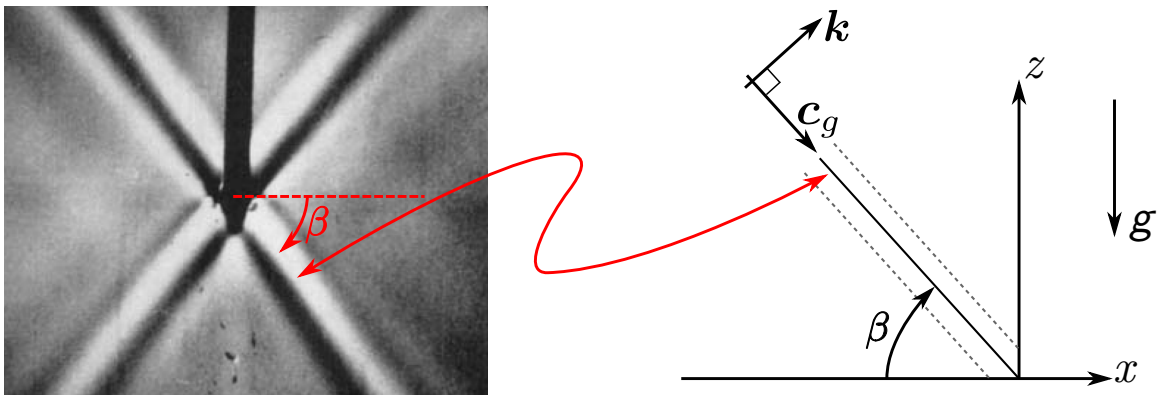

Figure 1-2: The image on the left is that of an internal gravity wave generated by the vertical oscillation of cylinder extended into the page [14]. The observed pattern of wave propagation is sometimes referred to as "St. Andrew's Cross". The vertical rod which supports the oscillating cylinder in the centre is visible as a dark shadow. The resulting beams emanate at an angle β to the horizontal. Following the beam that radiates towards the lower right corner, the image on the right indicates the directions of the group velocity $\boldsymbol{c}_g$ and phase velocity $\boldsymbol{c}$. Lines of constant phase are shown parallel to the group velocity.

$$\boldsymbol{c}_g \equiv \boldsymbol{\nabla}_k \, \omega = N \frac{m}{|\boldsymbol{k}|^3} \left\{ m \hat{\boldsymbol{e}}_x - k \hat{\boldsymbol{e}}_z \right\}. \tag{1.37b}$$

The group velocity and phase velocity are found to be perpendicular to one another, which equivalently implies the group velocity is also perpendicular to the wavevector,

$$\boldsymbol{c}_g \cdot \boldsymbol{c} = \boldsymbol{c}_g \cdot \boldsymbol{k} = 0. \tag{1.38}$$

This unusual relationship between the directions of $\boldsymbol{c}_g$ and $\boldsymbol{c}$ is attributed to the anisotropy of the system. The density stratification is unique to the direction of gravity resulting in a dispersion relation which requires that the frequency of oscillation is solely dependent on the orientation of the wavevector, independent of its magnitude. Also note that the vertical components are exactly opposite,

$$(\boldsymbol{c} + \boldsymbol{c}_g) \cdot \hat{\boldsymbol{e}}_z = 0. \tag{1.39}$$

This is a convenient property to keep in my mind when drawing the wavevector and group velocity; both vectors are orthogonal with opposing vertical directions.

Physically, the fluid motion is along lines of constant phase unlike the case of the more familiar surface waves. This is apparent by reconsidering the continuity equation (1.27b), which can be re-written for the plane wave solution as

$$\boldsymbol{k} \cdot \boldsymbol{u} = 0. \tag{1.40}$$

Revisiting the fully nonlinear governing equations (1.27) in view of the linear plane wave solution, we can expand the advective terms as

$$\boldsymbol{u} \cdot \boldsymbol{\nabla} = u\frac{\partial}{\partial x} + w\frac{\partial}{\partial z} = uk + wm. \tag{1.41}$$

By recognizing (1.41) is equivalent to (1.40), we find the remarkable result that the plane wave solution *is* the fully nonlinear solution since the nonlinear terms identically vanish [18]. We will return to this crucial point in our construction of wave beams in section §1.6. For now, we may calculate the other field variables in terms of w_0 by returning to (1.27),

$$\begin{Bmatrix} u \\ w \\ p \\ \rho \end{Bmatrix} = w_0 \begin{Bmatrix} -\frac{m}{k} \\ 1 \\ -\frac{\omega m \rho_0}{k^2} \\ \mathrm{i}\frac{N^2 \rho_0}{\omega g} \end{Bmatrix} \exp\left\{\mathrm{i}(kx + mz - \omega t)\right\}. \tag{1.42}$$

1.5 Energy flow rate

We may also consider the energy flow rate by manipulating the governing equations. Taking the dot product of the momentum equations (1.27a) with the velocity vector $\boldsymbol{u}$, and making use of (1.27b), returns

$$\frac{D}{Dt}\left\{\frac{1}{2}\rho_0\left[u^2 + v^2 + w^2\right]\right\} + g\rho w = -\boldsymbol{\nabla} \cdot (p\boldsymbol{u}). \tag{1.43}$$

Upon substituting the incompressible fluid equation (1.27c) for w in $g\rho w$, (1.43) can be rewritten and recognized as energy conservation

$$\frac{D}{Dt}\left\{\frac{1}{2}\rho_0\left[|\boldsymbol{u}|^2+\frac{N^2}{(d\overline{\rho}/dz)^2}\rho^2\right]\right\}=-\boldsymbol{\nabla}\cdot(p\boldsymbol{u})\,. \tag{1.44}$$

The velocity squared term will be recognized as the kinetic energy and the term involving density perturbations to the local density field is the potential energy due to gravity and buoyancy. The total time (material) derivative indicates that the change in mechanical energy is calculated with respect to a particular fluid parcel. Then we can interpret the divergence of the quantity $p\boldsymbol{u}$ as the time rate of change of the energy per unit volume following a fluid parcel. By integrating (1.44) over a volume, it becomes clear that the vector quantity $p\boldsymbol{u}$ is simply the energy flux rate through a boundary:

$$\int_V \boldsymbol{\nabla}\cdot(p\boldsymbol{u})\,\mathrm{d}V=\int_{A_{yz}} pu\,\mathrm{d}y\mathrm{d}z+\int_{A_{xz}} pv\,\mathrm{d}x\mathrm{d}z+\int_{A_{xy}} pw\,\mathrm{d}x\mathrm{d}y=\int_A p\boldsymbol{u}\cdot\,\mathrm{d}\boldsymbol{A}. \tag{1.45}$$

Because $\boldsymbol{A}$ points outwards, the negative sign on the right-hand side of (1.44) is consistent with the fact that a net outward flux of $p\boldsymbol{u}$, that is (1.45) > 0, equates to a loss in the total mechanical energy of the chosen volume of integration.

1.6 Wave beams

As mentioned at the end of §1.4, the plane wave solution is an exact solution because the advective terms vanish. This is so because the advective terms, $\boldsymbol{u}\cdot\boldsymbol{\nabla}$, account for spatial variations in the direction of the flow field; however internal waves are unique in that there is no spatial variation in this direction. This implies that plane waves of the same frequency ω and hence, via the dispersion relation (1.36), the same angle of propagation, do not interact with one another regardless the magnitude of the wavevector. This is shown explicitly by considering two plane waves with the same frequency ω,

$$\boldsymbol{u}=\boldsymbol{u}_{0,1}\mathrm{e}^{\mathrm{i}(\boldsymbol{k}_1\cdot\boldsymbol{x}-\omega t)}+\boldsymbol{u}_{0,2}\mathrm{e}^{\mathrm{i}(\boldsymbol{k}_2\cdot\boldsymbol{x}-\omega t)}. \tag{1.46}$$

The advective acceleration—for the arbitrarily chosen variable w—is

$$(\boldsymbol{u}\cdot\boldsymbol{\nabla})w = (u_1+u_2)(\mathrm{i}k_1w_1+\mathrm{i}k_2w_2)+(v_1+v_2)(\mathrm{i}l_1w_1+\mathrm{i}l_2w_2) \\ +(w_1+w_2)(\mathrm{i}m_1w_1+\mathrm{i}m_2w_2) \tag{1.47}$$

which can be more insightfully written as

$$(\boldsymbol{u}\cdot\boldsymbol{\nabla})w = \mathrm{i}w_1\underbrace{(\boldsymbol{k}_1\cdot\boldsymbol{u}_1)}_{0}+\mathrm{i}w_2\underbrace{(\boldsymbol{k}_2\cdot\boldsymbol{u}_2)}_{0}+\mathrm{i}\left\{w_1\left[\boldsymbol{k}_1\cdot\boldsymbol{u}_2\right]+w_2\left[\boldsymbol{k}_2\cdot\boldsymbol{u}_1\right]\right\} \tag{1.48}$$

The first two terms are zero by (1.40). Furthermore, by (1.36), the wavevectors $\boldsymbol{k}_1$ and $\boldsymbol{k}_2$ are parallel, as are the velocity vectors $\boldsymbol{u}_1$ and $\boldsymbol{u}_2$. Then by the same token, (1.40) requires the remaining two terms in (1.48) to vanish.

We can then superpose a number of plane waves with frequency ω as an integral sum, which is a so-called wave beam and is also an exact nonlinear solution [18]. To do so, we first introduce the cross-beam coordinate η which is directed along the wavevector $\boldsymbol{k}$,

$$\eta = x\sin\beta + y\cos\beta, \tag{1.49}$$

according to the second of figure 1-2. Foreseeing more difficult calculations to follow, it is worthwhile to introduce the streamfunction which satisfies (1.27b) by using $v=0$,

$$u = \frac{\partial\psi}{\partial z}, \quad w = -\frac{\partial\psi}{\partial x}. \tag{1.50}$$

The wave beam in terms of the streamfunction is

$$\psi(\eta,t) = \underbrace{\left\{\int_0^\infty \widehat{Q}(\kappa)\mathrm{e}^{\mathrm{i}\kappa\eta}\,\mathrm{d}\kappa\right\}}_{\equiv Q(\eta)}\mathrm{e}^{-\mathrm{i}\omega t}+\mathrm{c.c.}, \tag{1.51}$$

where κ is the magnitude of the wavevector—or simply the wavenumber, $\widehat{Q}(\kappa)$ is the complex amplitude of the plane wave with wavenumber κ, and the integral sum is defined as the η-dependence of the profile as $Q(\eta)$. We require $\widehat{Q}(\kappa)$ to be complex so that it accounts for the difference in phase associated with the plane waves. The

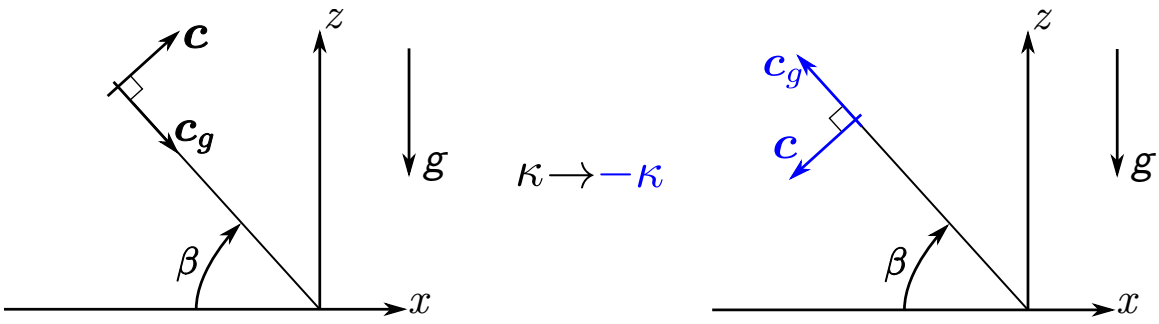

Figure 1-3: The effect of the sign of the magnitude of the wavevector κ when the direction η is fixed by the dispersion relation. Flipping the sign of κ also flips the direction of the group velocity $\boldsymbol{c}_g$ and phase velocity $\boldsymbol{c}$.

complex conjugate is included so that ψ is explicitly real and upcoming nonlinear calculations will be made more feasible.

The limits of integration are such that $\kappa > 0$ which is required for uni-directional beams [19]. To see this more clearly, consider $\kappa \to -\kappa$ as shown in figure 1-3. The group velocity and phase velocity of a plane wave with $-\kappa$ flip in direction by (1.37).

To understand how energy is transported by a wave beam, let us first average (1.45) over a period of wave oscillation, $2\pi/\omega$,

$$\mathscr{F} = \int_A \left\{ \frac{1}{2\pi/\omega} \int_0^{2\pi/\omega} p\boldsymbol{u} \, \mathrm{d}t \right\} \cdot \, \mathrm{d}\boldsymbol{A}. \tag{1.52}$$

The average energy flow rate, (1.52), can be calculated for beams in terms of the streamfunction profile $Q(\eta)$ by first writing the velocity profile as

$$\boldsymbol{u} = \frac{\partial \psi}{\partial z}\hat{\boldsymbol{e}}_x - \frac{\partial \psi}{\partial x}\hat{\boldsymbol{e}}_z = \{\cos\beta\hat{\boldsymbol{e}}_x - \sin\beta\hat{\boldsymbol{e}}_z\} \left(Q_\eta \mathrm{e}^{-\mathrm{i}\omega t} + \text{c.c.}\right), \tag{1.53}$$

where the notation $Q_\eta = dQ/d\eta$ is used. Since the beam comprises only of planes waves with the common frequency ω, the linearised equations (1.27) can be used to solve for the variation in pressure p with the resulting magnitude of $p\boldsymbol{u}$ being

$$p\,|\boldsymbol{u}| = \left\{N\rho_0 \cos\beta \left(\mathrm{i}Q\mathrm{e}^{-\mathrm{i}\omega t} + \text{c.c.}\right)\right\} \left\{Q_\eta \mathrm{e}^{\mathrm{i}\omega t} + \text{c.c.}\right\}. \tag{1.54}$$

Time averaging and writing (1.52) *per unit depth* into the uniform direction y, we find

$$\mathcal{F} = \mathrm{i}N\rho_0 \cos\beta \int_{-\infty}^{\infty} \left(QQ_\eta^* - Q^*Q_\eta\right)\, \mathrm{d}\eta = \mathrm{i}N\rho_0 \cos\beta \int_{-\infty}^{\infty} \left\{\left(QQ^*\right)_\eta - 2Q^*Q_\eta\right\}\, \mathrm{d}\eta \tag{1.55}$$

where the product rule $\left(QQ^*\right)_\eta = Q_\eta Q^* + QQ_\eta^*$ was employed in reverse. The term $\left(QQ^*\right)_\eta$ vanishes when integrated over the limits $\eta \to \pm\infty$ since Q represents a beam of finite thickness, $Q(\eta \to \pm\infty) \to 0$. Furthermore, the term Q^*Q_η can be nicely simplified within the spatial integration by considering Q in its integral form (1.51),

$$\begin{aligned}\int_{-\infty}^{\infty} Q^*Q_\eta\, \mathrm{d}\eta &= \int_{-\infty}^{\infty} \left\{ \left(\int_0^{\infty} \widehat{Q}^*(\kappa)\mathrm{e}^{-\mathrm{i}\kappa\eta}\, \mathrm{d}\kappa \right) \left(\int_0^{\infty} \mathrm{i}\overline{\kappa}\widehat{Q}(\overline{\kappa})\mathrm{e}^{\mathrm{i}\overline{\kappa}\eta}\, \mathrm{d}\overline{\kappa} \right) \right\}\, \mathrm{d}\eta \\ &= \int_0^{\infty}\int_0^{\infty} \left\{ \int_{-\infty}^{\infty} \mathrm{i}\overline{\kappa}\widehat{Q}(\overline{\kappa})\widehat{Q}^*(\kappa)\mathrm{e}^{\mathrm{i}\eta(\overline{\kappa}-\kappa)}\, \mathrm{d}\eta \right\}\, \mathrm{d}\overline{\kappa}\mathrm{d}\kappa. \end{aligned} \tag{1.56}$$

It is convenient to first integrate over η and make use of the Dirac delta function, δ, which exposes itself by the definition

$$\delta(\overline{\kappa} - \kappa) \equiv \frac{1}{2\pi} \int_{-\infty}^{\infty} \mathrm{e}^{\mathrm{i}\eta(\overline{\kappa}-\kappa)}\, \mathrm{d}\eta. \tag{1.57}$$

Implementing (1.57) simplifies (1.56) to

$$\int_{-\infty}^{\infty} Q^*Q_\eta\, \mathrm{d}\eta = \mathrm{i}2\pi \int_0^{\infty}\int_0^{\infty} \left\{\mathrm{i}\overline{\kappa}\widehat{Q}(\overline{\kappa})\widehat{Q}^*(\kappa)\delta\left(\overline{\kappa} - \kappa\right)\right\}\, \mathrm{d}\overline{\kappa}\mathrm{d}\kappa. \tag{1.58}$$

Integrating over $\overline{\kappa}$, aided by the factor $\delta(\overline{\kappa} - \kappa)$, and then noting that the modulus of the complex quantity is $\widehat{Q}\widehat{Q}^* = \left|\widehat{Q}\right|^2$, (1.55) finally becomes

$$\mathcal{F} = 4\pi N\rho_0 \cos\beta \int_0^{\infty} \kappa \left|\widehat{Q}(\kappa)\right|^2\, \mathrm{d}\kappa. \tag{1.59}$$

The expression (1.59) is the average energy flow rate per unit depth that will be used to evaluate the strength of wave beams.

Chapter 2

Oblique reflections of internal gravity wave beams

Having now a working knowledge of internal gravity wave beams, it is desirable to understand their interactions within their environment. One such interaction is that with topography. A propagating wave beam will carry energy across the seas, but what happens when a beam finds its path obstructed by natural barriers such as cliffs and ridges, or more specifically, how is the energy flow redirected? Within the limit of weakly nonlinear analysis, the answer to the preceding question is the subject of this chapter.

2.1 Motivating the weakly nonlinear model

Bell (1975) [1] first made an analytical investigation into the generation mechanism of internal gravity waves by a simple harmonic flow, as a model for tidal flow, in a stratified medium of infinite depth over an obstacle. The study found that waves of frequency equal to harmonics of the tidal flow—below the limiting Brunt-Väisälä frequency—are generated and radiated outwards in a cross pattern. Lamb (2004) [11] revisited the problem by means of numerical simulations, though with a finite depth imposed by an upper boundary. This generation mechanism is illustrated in figure 2-1 [19] in which beams radiate from the generation site near the centre of

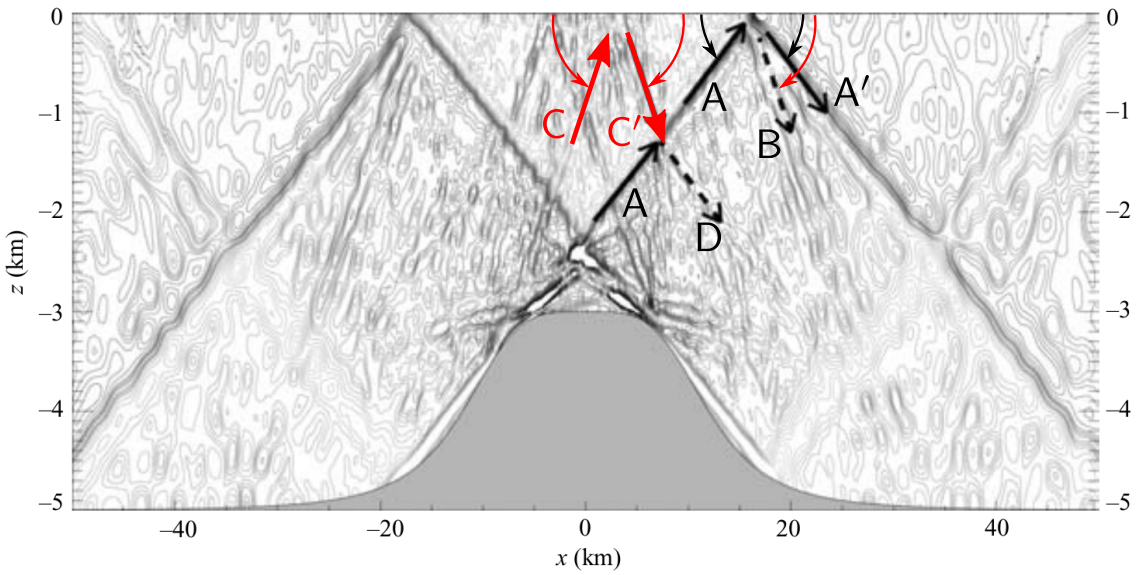

Figure 2-1: Contour plot of the horizontal velocity field generated by a two-dimensional CFD simulation. The background flow is oscillatory which generates beams over the ridge. Beams that are generated by nonlinear interactions are shown in dashed arrows. A second-harmonic beam generated by the tidal flow, C, is shown in red. It tuns out to have the same frequency as the secondary reflected beam B, which suggests that the reflections of internal gravity wave beams may be treated as a weakly nonlinear interactions which can give rise to second- (and higher-) harmonics. [19]

the image. Let us focus our attention here where a solid arrow marks the beam A, of the fundamental frequency which is to say that it has the same frequency as the tidal flow, and propagates towards the top-right corner. Following this beam, we find it encounters the upper boundary and reflects into two beams. The first, A′, propagating towards the bottom-right corner, retains the angle to the horizontal and thus by the dispersion relation (1.36) also propagates with the same frequency. We will shortly return to the secondly generated beam, B, that is marked by a dashed arrow.

Repaying a visit to the beams generated over the topography, we also find second-harmonics that have twice the frequency of the tidal flow. The reflection of a second-harmonic beam, indicated in red and labelled C, is marked as beam C′ and appears to have the same angle of propagation from the horizontal as the beam B generated from the reflection of the primary-harmonic A. The fact that beams C′ and B travel

with the same angle, the dispersion relation requires they have the same frequency. Specifically, the reflection of a primary-harmonic gives rise to higher order harmonics that have frequency less than the Brunt-Väisälä frequency. This observation strongly intimates that weakly nonlinear interactions are at play here since the quadratic nonlinear advective terms can explain the presence of second-harmonic beams.

The beam D generated by the collision of beam A with C' can also be explained in terms of weak nonlinearities [19]. The analysis that follows, however, will focus on the understanding of reflections.

The prediction by Phillips [16] mentioned in §1.1 is evident here since the reflected beam A' has the same angle of propagation as the incident beam A. Although here we have only shown a reflection from a horizontal plane in figure 2-1, recall from §1.1 that some attention has been directed towards the more general case of reflections from an inclined slope; such are the interactions expected to occur as internal waves propagate toward the non-uniform sea floor. Much of the previous work on the reflections of internal waves have investigated the particular case in which the incoming beam is normal to the slope [3, 8, 15, 19, 21], so that the problem of interest is two-dimensional since the incoming beam is in the same vertical as the slope; they are both uniform along the same coordinate. Here, we wish to extend the analysis of reflections to incorporate the case that allows the incoming beam to be in a vertical plane oblique relative to the uniform slope as shown in figure 2-2.

2.2 Governing equations

From this point forward, we will return to the non-dimensional formulation of the governing equations presented at the end of §1.3 and reproduced here for convenience,

$$\left(\frac{\partial}{\partial t} + \boldsymbol{u}\cdot\boldsymbol{\nabla}\right)\boldsymbol{u} = -\boldsymbol{\nabla}p - \rho\hat{\boldsymbol{e}}_z, \tag{2.1a}$$

$$\boldsymbol{\nabla}\cdot\boldsymbol{u} = 0, \tag{2.1b}$$

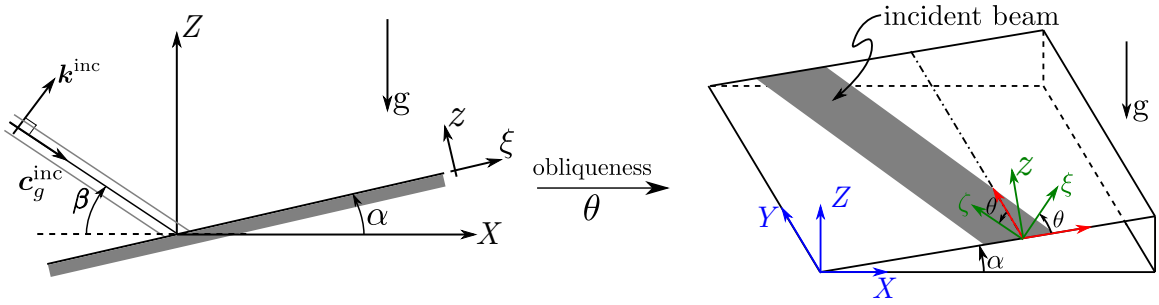

Figure 2-2: Visualizing the geometry of reflections from a slope. The figure on the left shows the simpler case of an incoming beam uniform to the slope. Both, the incoming beam and the uniform slope lie in the same vertical plane and are both uniform into the page. The figure on the right introduces a relative obliqueness θ between the beam and the slope—indicated by its grey-shaded trace, which is measured relative to the dot-dashed line. In this case, the beam is uniform in ζ and the slope is uniform in Y.

$$\left(\frac{\partial}{\partial t} + \boldsymbol{u}\cdot\boldsymbol{\nabla}\right)\rho = w. \tag{2.1c}$$

Applied to the problem of interest here, we first draw the geometry of reflections in greater detail as shown in figure 2-2. In the case of a plane reflection, the incoming beam is uniform in the page as is the slope. The coordinates (ξ, z) are useful since the boundary condition prohibits flow normal to the slope (in z) along the slope ($z = 0$). We look for similar convenience in the case of relative obliqueness, θ, between the beam and the slope. Now, the incident wave beam is uniform in ζ and the slope is uniform in Y; the two being related by θ. In effect, we have rotated the beam by an angle θ in z, normal to the slope, leaving the slope unchanged. The coordinate system (ξ, ζ, z) takes advantage of the uniformity of the beam in ζ so that $\partial/\partial\zeta = 0$. In particular, we can introduce the streamfunction ψ defined by the velocity field

$$u = \frac{\partial\psi}{\partial z}, \quad w = -\frac{\partial\psi}{\partial\xi}, \quad v = v(\xi, z, t), \tag{2.2a}$$

$$\boldsymbol{u} = u\hat{\boldsymbol{e}}_\xi + v\hat{\boldsymbol{e}}_\zeta + w\hat{\boldsymbol{e}}_z. \tag{2.2b}$$

Note that the velocity vector in (2.2) has been redefined from (1.8) introduced in §1.3.

The coordinate transformation requires the substitution

$$\hat{\boldsymbol{e}}_z \to (\cos\theta\sin\alpha)\hat{\boldsymbol{e}}_\xi - (\sin\theta\sin\alpha)\hat{\boldsymbol{e}}_\zeta + (\cos\alpha)\hat{\boldsymbol{e}}_z,$$
$$w \to (\cos\theta\sin\alpha)u - (\sin\theta\sin\alpha)v + (\cos\alpha)w,$$

Pressure is subsequently eliminated in a fashion similar to the treatment presented in §1.4 by considering only the ζ-momentum, ζ-vorticity, and incompressibility equations. Recall that the vorticity is defined as $\boldsymbol{\nabla}\times\boldsymbol{u}$; and the ζ-vorticity is $\partial u/\partial z - \partial w/\partial\xi = \nabla^2\psi$ where the Laplacian is in the plane normal to the beam,

$$\nabla^2 = \frac{\partial}{\partial\xi^2} + \frac{\partial^2}{\partial z^2}. \tag{2.3}$$

If we then continue our manipulation of the governing equations with the substitution (2.2a) in favour of ψ, (2.1) becomes

$$\zeta\text{-momentum:} \qquad v_t + J(v,\psi) - \rho\sin\alpha\sin\theta = 0, \tag{2.4a}$$
$$\zeta\text{-vorticity:} \qquad \left(\nabla^2\psi\right)_t + J\left(\nabla^2\psi,\psi\right) + \rho_z\sin\alpha\cos\theta - \rho_\xi\cos\alpha = 0, \tag{2.4b}$$
$$\text{incompressibility:} \qquad \rho_t + J(\rho,\psi) - \psi_z\sin\alpha\cos\theta + \psi_\xi\cos\alpha + v\sin\alpha\sin\theta = 0, \tag{2.4c}$$

where we have again adopted the notation $f_{t,\xi,z} \equiv \partial f/\partial(t,\xi,z)$ to denote derivatives. Here the Jacobian is calculated as $J(a,b) \equiv a_\xi b_z - a_z b_\xi$ and represents the advective term since $(\boldsymbol{u}\cdot\boldsymbol{\nabla})f = J(f,\psi)$. Take for example, the second term $J(v,\psi)$ in (2.4a). Physically, this is the gradient of the ζ-velocity, v, taken in the direction of the velocity flow field $\boldsymbol{u}$ and has the same meaning as the quantity $(\boldsymbol{u}\cdot\boldsymbol{\nabla})v$.

We have patiently endured some few pages of algebra in deriving the set (2.4) without gaining much insight into the question of wave beams reflecting from a slope, but let us too reflect on what has been accomplished thus far. Upon comparing the relatively unmodified equations (2.1) to (2.4), it becomes clear that we have reduced our mathematical problem of 5 partial differential equations of 5 variables to 3 of each: pressure has been eliminated by directly engaging the uniformity of

the incident beam in the ζ-direction and also considering vorticity elsewhere; and the ξ, z-velocities have been displaced in favour of the streamfunction ψ which satisfies the continuity equation by definition, hence $\boldsymbol{\nabla} \cdot \boldsymbol{u} = 0$ is not a part of (2.4). Per (1.59), we can calculate the strength of any beam knowing the streamfunction alone, relieving ourselves of the duty to further determine the exact velocities of the flow field. To solve (2.4), we now turn to the analytical methods of weakly nonlinear theory.

2.3 Weakly nonlinear expansions

For weakly nonlinear wave beams, we make the expansions

$$\begin{Bmatrix} \psi \\ \rho \\ v \end{Bmatrix} = \epsilon \begin{Bmatrix} Q(\xi,z)\mathrm{e}^{-\mathrm{i}\omega t} + \text{c.c.} \\ R(\xi,z)\mathrm{e}^{-\mathrm{i}\omega t} + \text{c.c.} \\ V(\xi,z)\mathrm{e}^{-\mathrm{i}\omega t} + \text{c.c.} \end{Bmatrix} + \epsilon^2 \begin{Bmatrix} Q_0(\xi,z) + \left[Q_2(\xi,z)\mathrm{e}^{-2\mathrm{i}\omega t} + \text{c.c.}\right] \\ R_0(\xi,z) + \left[R_2(\xi,z)\mathrm{e}^{-2\mathrm{i}\omega t} + \text{c.c.}\right] \\ V_0(\xi,z) + \left[V_2(\xi,z)\mathrm{e}^{-2\mathrm{i}\omega t} + \text{c.c.}\right] \end{Bmatrix} + \cdots \quad (2.5)$$

where $\epsilon \ll 1$ is a small-scaling parameter which allows us to separate solutions of (2.4) based on their orders of magnitude. Specifically, all terms of ϵ satisfy (2.4) as do all terms of ϵ^2 in a distinguished fashion.

The physical meaning of ϵ deserves some care so that we are consistent in our understanding and can compare our analysis to experiments, field observations, and computational simulations. The wave beams consist of two separable parts, the time-dependent oscillations, and the amplitude associated with the spatial configuration. The first-order solution of $\mathcal{O}(\epsilon)$ includes the spectral density of the incident beam as expressed in (2.7) of §2.3.1. The velocity field is more readily associated with the physics of the flow and can be expressed as $\partial\psi/\partial\eta$, where η is the cross-beam coordinate as discussed in §1.6. Given some beam profile, by measurement in the field or assignment in computation, it must first be non-dimensionalized by the factor g/N ([=]m/s) and then scaled by the maximum value of the velocity profile upon comparison with velocity field represented by the streamfunction (2.7). An example of the beam assignment in terms of the cross-beam coordinate (1.51), and its relation

to the more suitable form for analysis (2.7), will be demonstrated in §3.1.

The expansions take the form of (2.5) in our anticipation of the types of interactions that can occur due to quadratic nonlinearities. Terms like Q_0 describe a mean flow which lack time dependency and arise from products of $\mathcal{O}(\epsilon)$ terms having the form QQ^*. Second-harmonic flows are indicated by the subscript '2', which have twice the frequency of the incident beam and arise from QQ kinds of interactions. Of course, we can continue our expansions indefinitely in which each higher-order term has a smaller amplitude as has been done for the plane reflections [19]; however here we are primarily concerned with the effect of obliqueness on the dominant nonlinear terms, which are of $\mathcal{O}(\epsilon^2)$.

2.3.1 Linear solution, $\mathcal{O}(\epsilon)$

The first order term, $\psi = \epsilon\left\{Q\mathrm{e}^{-\mathrm{i}\omega t} + \text{c.c.}\right\}$, is a simple sum of the incident and reflected beam

$$Q(\xi, z) = Q^{\text{inc}}(\xi, z) + Q^{\text{ref}}(\xi, z), \tag{2.6}$$

where spatial profiles in Q are the integral expressions

$$Q^{\text{inc}}(\xi, z) = \int_0^\infty A(l)\mathrm{e}^{\mathrm{i}l\left(\xi + m^{\text{inc}}z\right)}\,\mathrm{d}l, \tag{2.7}$$

$$Q^{\text{ref}}(\xi, z) = \int_0^\infty A^{\text{ref}}(l^{\text{ref}})\mathrm{e}^{\mathrm{i}l^{\text{ref}}\left(\xi + m^{\text{ref}}z\right)}\,\mathrm{d}l^{\text{ref}}. \tag{2.8}$$

We perform the integral over the ξ-wavenumber where m^{inc} and m^{ref} are constant geometric factors, which describe the direction of propagation in (ξ, z), respective to each beam and will soon be determined by enforcing the dispersion relation. We would like to calculate all the flow variables in terms of the incident beam profile, Q^{inc}.

The boundary condition is simply that the flow does not penetrate the topography, or more precisely that the velocity component normal to the slope, w, is exactly zero

everywhere on the slope at all times,

$$w|_{z=0} = -\frac{\partial \psi}{\partial \xi}\bigg|_{z=0} = 0 \text{ for all } \xi \text{ and } t. \tag{2.9}$$

Upon application of (2.9) to (2.6), we find that $l^{\text{ref}} = l$ and $A^{\text{ref}} = -A$ so

$$Q^{\text{ref}}(\xi, z) = -\int_0^\infty A(l) \mathrm{e}^{\mathrm{i}l\left(\xi + m^{\text{ref}} z\right)} \, \mathrm{d}l, \tag{2.10}$$

and for completeness we also rewrite (2.6) as

$$Q(\xi, z) = \int_0^\infty A(l) \mathrm{e}^{\mathrm{i}l\xi} \left[\mathrm{e}^{ilm^{\text{inc}} z} - \mathrm{e}^{ilm^{\text{ref}} z}\right] \, \mathrm{d}l. \tag{2.11}$$

Substituting the expansion (2.5) into the governing equations (2.4) and collecting $\mathcal{O}(\epsilon)$ terms followed by $\mathrm{e}^{-\mathrm{i}\omega t}$ terms, we find from (2.4a) and (2.4c) that R and V can be expressed in terms of Q derivatives,

$$R = \mathrm{i}\omega \frac{Q_z \sin\alpha \cos\theta - Q_\xi \cos\alpha}{\omega^2 - \sin^2\alpha \sin^2\theta}, \tag{2.12a}$$

$$V = -\sin\alpha \sin\theta \frac{Q_z \sin\alpha \cos\theta - Q_\xi \cos\alpha}{\omega^2 - \sin^2\alpha \sin^2\theta}. \tag{2.12b}$$

Substituting the results (2.12) into ζ-vorticity (2.4b) yields

$$\begin{aligned} -\mathrm{i}\omega \left(Q_{\xi\xi} + Q_{zz}\right) + \frac{\mathrm{i}\omega}{\omega^2 - \sin^2\alpha \sin^2\theta} \Big[& \sin\alpha \cos\theta \left(Q_{zz} \sin\alpha \cos\theta - Q_{\xi z} \cos\alpha\right) \\ & - \cos\alpha \left(Q_{z\xi} \sin\alpha \cos\theta - Q_{\xi\xi} \cos\alpha\right) \Big] = 0. \end{aligned} \tag{2.13}$$

Upon implementing (2.11) and the dispersion relation $\omega = \sin\beta$ into (2.13), and then collecting like exponentials, $\exp\left(\mathrm{i}lm^{\text{inc}} z\right)$ and $\exp\left(\mathrm{i}lm^{\text{ref}} z\right)$, we find m^{inc} and m^{ref}

satisfy the same quadratic equation

$$m^{\pm} = \frac{-2\cos\alpha\sin\alpha\cos\theta \pm \sqrt{\lambda}}{2\left(\sin^2\beta - \sin^2\alpha\right)} \tag{2.14}$$

where

$$\lambda \equiv \left(4\cos^2\alpha\sin^2\alpha\cos^2\theta\right) - 4\left(\sin^2\beta - \sin^2\alpha\right)\left(\sin^2\beta - \sin^2\alpha\sin^2\theta - \cos^2\theta\right). \tag{2.15}$$

Requiring m real, then $\lambda > 0$ and

$$\cos^2\alpha\sin^2\alpha\cos^2\theta > \left(\sin^2\beta - \sin^2\alpha\right)\left(\sin^2\beta - \sin^2\alpha\sin^2\theta - \cos^2\theta\right).$$

Expanding the right-hand side,

$$0 > \sin^4\beta - \sin^2\beta\left[\sin^2\theta + \sin^2\alpha + \cos^2\alpha\cos^2\theta\right] + \sin^2\alpha\sin^2\theta,$$

and finally using the identities $\cos^2\alpha\cos^2\theta = (1-\sin^2\alpha)(1-\sin^2\theta)$, we find the restriction in terms of the simple inequality

$$\sin^2\beta > \sin^2\beta\sin^2\alpha. \tag{2.16}$$

The meaning of this restriction is the subject of appendix A.

Provided (2.16) is met,

$$\lambda = 4\cos^2\beta(\sin^2\beta - \sin^2\alpha\sin^2\theta) > 0 \tag{2.17}$$

and (2.14) is simplified to

$$m^{\pm} = -\cos\theta\frac{\cos\alpha\sin\alpha \mp r\cos\beta\sin\beta}{\sin^2\beta - \sin^2\alpha}, \tag{2.18}$$

where

$$r \equiv \sqrt{1 + \tan^2\theta\left(1 - \frac{\sin^2\alpha}{\sin^2\beta}\right)}. \tag{2.19}$$

To determine which sign of $\pm$ in (2.18) corresponds to which beam, either incident or reflected, consider the plane reflection by taking the limit $\theta \to 0$, in which case $\cos\theta \to 1$ and $r \to 1$. Introducing trigonometric identities into the numerator,

$$\cos\alpha \sin\alpha \mp \cos\beta \sin\beta = \frac{1}{2}\left(\sin 2\alpha \mp \sin 2\beta\right) = \cos(\alpha \pm \beta)\sin\left(\alpha \mp \beta\right),$$

and the denominator,

$$\begin{aligned}\sin\beta \sin\beta - \sin\alpha \sin\alpha &= \left[\frac{1}{2}(1-\cos 2\beta)\right] - \left[\frac{1}{2}(1-\cos 2\alpha)\right] = \frac{1}{2}(\cos 2\alpha - \cos 2\beta) \\ &= \frac{1}{2}\left[-2\sin(\alpha+\beta)\sin(\alpha-\beta)\right] = -\sin(\alpha+\beta)\sin(\alpha-\beta),\end{aligned}$$

we find

$$m_0^+ = \cot(\alpha - \beta), \tag{2.20a}$$

$$m_0^- = \cot(\alpha + \beta). \tag{2.20b}$$

If we now assume $\beta > \alpha$, the wavevectors of the incident $\left(\boldsymbol{k}^{\text{inc}}\right)$ and reflected $\left(\boldsymbol{k}^{\text{ref}}\right)$ beams relative to the slope can be drawn as shown in figure 2-3. Matching these wavevectors with the two possibilities,

$$\boldsymbol{k}_0^+ = l\left\{\hat{\boldsymbol{e}}_\xi + \cot(\alpha-\beta)\hat{\boldsymbol{e}}_z\right\}, \qquad \left(\boldsymbol{k}_0^+ \cdot \hat{\boldsymbol{e}}_z < 0\right) \tag{2.21a}$$

$$\boldsymbol{k}_0^- = l\left\{\hat{\boldsymbol{e}}_\xi + \cot(\alpha+\beta)\hat{\boldsymbol{e}}_z\right\}, \qquad \left(\boldsymbol{k}_0^- \cdot \hat{\boldsymbol{e}}_z > 0\right) \tag{2.21b}$$

we determine based on the sign of the z-component of the wavevector that $\boldsymbol{k}_0^{\text{inc}} = \boldsymbol{k}_0^-$ and $\boldsymbol{k}_0^{\text{ref}} = \boldsymbol{k}_0^+$, implying that in general,

$$m^{\text{inc}} = m^- = -\cos\theta \frac{\cos\alpha\sin\alpha - r\cos\beta\sin\beta}{\sin^2\beta - \sin^2\alpha}, \tag{2.22a}$$

$$m^{\text{ref}} = m^+ = -\cos\theta \frac{\cos\alpha\sin\alpha + r\cos\beta\sin\beta}{\sin^2\beta - \sin^2\alpha}. \tag{2.22b}$$

These results agree with Tabaei et al. [19].

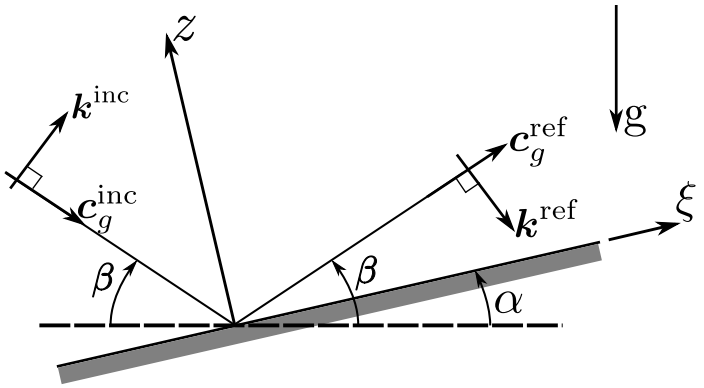

Figure 2-3: The geometry of the wavevectors in the case of plane reflection with $\beta > \alpha$. The incident beam has wavevector component positive in z whereas the reflected beam has negative wavevector component in z.

The linear solution is now complete; Q^{ref} is known according to (2.10) for any arbitrary spectral profile of the incident beam, $A(l)$. Furthermore, we can easily calculate the velocity field by (2.2a); as a particular example we show the spatial dependence of the velocity along ξ,

$$U(\xi, z) = \frac{\partial Q}{\partial z} = \int_0^\infty A(l) \mathrm{e}^{\mathrm{i}l\xi} \mathrm{i}l \left[m^{\mathrm{inc}} \mathrm{e}^{ilm^{\mathrm{inc}}z} - m^{\mathrm{ref}} \mathrm{e}^{ilm^{\mathrm{ref}}z} \right] \mathrm{d}l. \tag{2.23}$$

Notice that when $\beta \to \alpha$, $m^{\mathrm{ref}} \to \infty$ which is most clearly seen in the case of a normal reflection (2.20). The linear solution predicts a singular steady-state solution when the angle of propagation is the same as the angle of the slope. To understand why this happens, consider the kinematics relating the thickness of the incoming beam to the reflected beam as shown in figure 2-4. The thickness of each beam is related by the trace, d, over the slope. Resolving the geometry in terms of the incoming and reflected beam,

$$d^{\mathrm{inc}} = d \cos \phi^{\mathrm{inc}} = d \cos \left[\frac{\pi}{2} - (\beta + \alpha) \right] = d \sin(\beta + \alpha), \tag{2.24}$$

$$d^{\mathrm{ref}} = d \sin \phi^{\mathrm{ref}} = d \sin(\beta - \alpha). \tag{2.25}$$

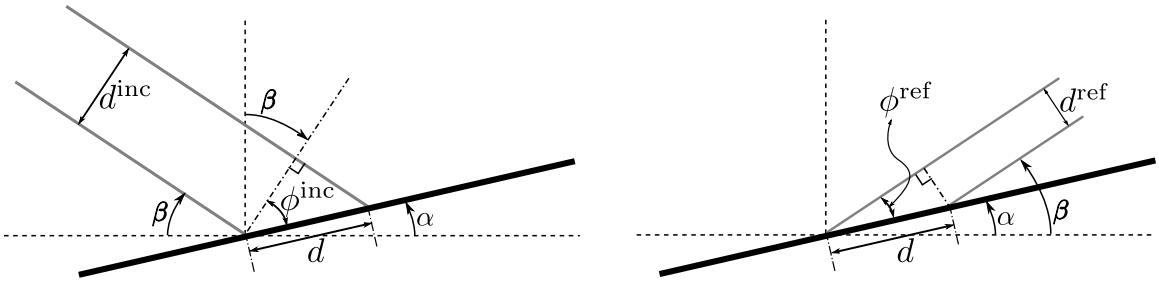

Figure 2-4: Kinematics of beam thickness. The diagram on the left illustrates the geometry of the incident beam with angle of propagation β from the horizontal normal to a slope of angle α. The thickness of the beam is given as d^{inc} and can be related to the trace of the incidence, d, which is common to the reflected beam and shown on the diagram to the right. Since the angle of propagation is maintained, as required by the boundary condition, the relationship between the incoming and reflected beam for a normal reflection is found to be $d^{\text{ref}}/d^{\text{inc}} = \sin(\beta - \alpha)/\sin(\beta + \alpha)$.

Then the thickness of the reflected beam can be expressed as

$$d^{\text{ref}} = d^{\text{inc}} \frac{\sin(\beta - \alpha)}{\sin(\beta + \alpha)}. \tag{2.26}$$

When we take the case $\beta \to \alpha$, we find $d^{\text{ref}} \to 0$. The reflected beam becomes infinitesimally thin and yet must carry a finite quantity of energy away from the reflection site. The distribution of a finite quantity over infinitesimal space is the cause of the singularity. A model which incorporates finite amplitude and viscous effects in this regime may provide a more accurate solution for the case $\beta \approx \alpha$ [3].

2.3.2 Mean flow, $\mathcal{O}(\epsilon^2)$

When we determined the linear solution (2.12), we collected $\mathcal{O}(\epsilon)$ terms after applying the expansion (2.5) to the governing equations (2.4). Now, we collect $\mathcal{O}(\epsilon^2)$ terms and notice there are exponential terms ($\mathrm{e}^{\pm \mathrm{i}2\omega t}$), due to QQ and Q^*Q^* interactions, and time-independent terms (e^0), due to QQ^* interactions. However, note that the time-independent terms represent the mean flow which *does not radiate in the far-field*. This flow does not transport energy away from the reflection site.

Gathering appropriate terms in (2.4a), we find

$$\langle J(v,\psi)\big|_{\epsilon^2}\rangle - R_0 \sin\alpha \sin\theta = 0, \tag{2.27}$$

where the time-average of the $\mathcal{O}(\epsilon^2)$ Jacobian is

$$\langle J(v,\psi)\big|_{\epsilon^2}\rangle = V_\xi Q^*_z - V_z Q^*_\xi + \text{c.c.} = J(V,Q^*) + \text{c.c.}. \tag{2.28}$$

Making use of the linear solution for V in terms of Q, (2.12b), the mean density is

$$R_0 = \frac{J(Q_\xi,Q^*)\cos\alpha - J(Q_z,Q^*)\sin\alpha\cos\theta}{\omega^2 - \sin^2\alpha\sin^2\theta} + \text{c.c.}. \tag{2.29}$$

Performing the same procedure on (2.4b),

$$\left\langle J(\nabla^2\psi,\psi)\big|_{\epsilon^2}\right\rangle + \left(\sin\alpha\cos\theta\frac{\partial}{\partial z} - \cos\alpha\frac{\partial}{\partial\xi}\right) R_0 = 0. \tag{2.30}$$

The only mean variable here is density—the same as in (2.27); we cannot expect any new information by pursuing this calculation and anticipate that doing so will only reproduce (2.29). Nonetheless, an effort is made to verify this expectation by first expanding the mean $\mathcal{O}(\epsilon^2)$ terms as before, $\langle J(\nabla^2\psi,\psi)\big|_{\epsilon^2}\rangle = J(\nabla^2 Q, Q^*) + \text{c.c.}$ and then substituting the expression (2.13) for $\nabla^2 Q$ so that

$$\begin{aligned} J(\nabla^2 Q, Q^*) + \text{c.c.} = \\ \frac{-1}{\omega^2 - \sin^2\alpha\sin^2\theta}\Bigg\{\Bigg[\overbrace{J(Q_{z\xi},Q^*)}^{\mathsf{A}}\sin\alpha\cos\theta - \overbrace{J(Q_{\xi\xi},Q^*)}^{\mathsf{B}}\cos\alpha\Bigg]\cos\alpha \\ - \Bigg[\underbrace{J(Q_{zz},Q^*)}_{\mathsf{C}}\sin\alpha\cos\theta - \underbrace{J(Q_{\xi z},Q^*)}_{\mathsf{D}}\cos\alpha\Bigg]\sin\alpha\cos\theta\Bigg\} + \text{c.c.}. \end{aligned} \tag{2.31}$$

The indicated Jacobians can be expanded by the product rule of calculus,

$$\mathsf{A} \to \frac{\partial}{\partial z}J(Q_\xi,Q^*) - J(Q_\xi,Q^*_z), \qquad \mathsf{B} \to \frac{\partial}{\partial\xi}J(Q_\xi,Q^*) - J(Q_\xi,Q^*_\xi),$$

$$\mathsf{C} \to \frac{\partial}{\partial z} J(Q_z, Q^*) - J(Q_z, Q_z^*), \qquad \mathsf{D} \to \frac{\partial}{\partial \xi} J(Q_z, Q^*) - J(Q_z, Q_\xi^*).$$

The second terms of A and D cancel each others complex conjugates, and the second terms of B and C cancel their own complex conjugates. Collecting like terms reveals a more compatible form of (2.31) with (2.30),

$$J(\nabla^2 Q, Q^*) + \text{c.c.} = \left(\sin\alpha\cos\theta\frac{\partial}{\partial z} - \cos\alpha\frac{\partial}{\partial \xi}\right) \frac{J(Q_z, Q^*)\sin\alpha\cos\theta - J(Q_\xi, Q^*)\cos\alpha}{\omega^2 - \sin^2\alpha\sin^2\theta} + \text{c.c.}, \tag{2.32}$$

and taken with the ζ-vorticity (2.30) returns (2.29) as before, supporting our earlier claim that (2.4a) and (2.4b) contain the same information with regards to the mean flow.

Before moving on, let us mention that the velocity profile is determined by the two variables Q_0 and V_0, although there remains only one more equation from our formulation (2.4) to consider. However, we remark that the remaining equation, the incompressibility condition (2.4c), includes *only* the vertical velocity component in $\hat{\boldsymbol{e}}_Z$ per (1.26c). Inspired by this observation, we will briefly return to the original coordinates (X, Y, Z). The velocity field in these coordinates is

$$\overline{\boldsymbol{U}} = \overline{U}\hat{\boldsymbol{e}}_X + \overline{V}\hat{\boldsymbol{e}}_Y + \overline{W}\hat{\boldsymbol{e}}_Z, \tag{2.33}$$

and the mean velocity will be designated with the subscript '0', so that $\overline{\boldsymbol{U}}_0$ is consistent in notation with (2.5). Written in terms of the velocity components in (ξ, ζ, z),

$$\boldsymbol{u} = \frac{\partial Q}{\partial z}\hat{\boldsymbol{e}}_\xi + V\hat{\boldsymbol{e}}_\zeta - \frac{\partial Q}{\partial \xi}\hat{\boldsymbol{e}}_z, \tag{2.34}$$

we find the vector components in (2.33) are

$$\overline{U} = \frac{\partial Q}{\partial z}\cos\theta\cos\alpha + \frac{\partial Q}{\partial \xi}\sin\alpha - V\sin\theta\cos\alpha \tag{2.35a}$$

$$\overline{V} = \frac{\partial Q}{\partial z}\sin\theta + V\cos\theta \tag{2.35b}$$

$$\overline{W} = \frac{\partial Q}{\partial z}\cos\theta\sin\alpha - \frac{\partial Q}{\partial \xi}\cos\alpha - V\sin\theta\sin\alpha \tag{2.35c}$$

in accordance with figure 2-2. The standard procedure to make the coordinate transformation is outlined in part of appendix A.

In light of (2.35), it is clear that the time-averaged $\mathcal{O}(\epsilon^2)$ incompressibility equation (2.4c), which reads

$$\langle J(\rho,\psi)|_{\epsilon^2}\rangle - \frac{\partial Q_0}{\partial z}\sin\alpha\cos\theta + \frac{\partial Q_0}{\partial \xi}\cos\alpha + V_0\sin\alpha\sin\theta = 0, \tag{2.36}$$

can be more succinctly written as

$$\overline{W}_0 = \langle J(\rho,\psi)|_{\epsilon^2}\rangle\,. \tag{2.37}$$

The quadratic forcing is found just as before in (2.28) with the linear solution of R from (2.12a),

$$\begin{aligned}\langle J(\rho,\psi)|_{\epsilon^2}\rangle &= J(R,Q^*) + \text{c.c.}\\ &= \frac{\mathrm{i}\omega\left[(J(Q_z,Q^*)\sin\alpha\cos\theta - J(Q_\xi,Q^*)\cos\alpha\right]}{\omega^2 - \sin^2\alpha\sin^2\theta} + \text{c.c.}\end{aligned} \tag{2.38}$$

The Jacobians here can be combined with their complex conjugates by

$$\begin{aligned}\mathrm{i}\left\{J(Q_z,Q^*) - J(Q_z^*,Q)\right\} &= \mathrm{i}\left\{\left[\frac{\partial}{\partial z}J(Q,Q^*) - \cancel{J(Q,Q_z^*)}\right] - \cancel{J(Q_z^*,Q)}\right\}\\ &= \mathrm{i}\frac{\partial}{\partial z}J(Q,Q^*).\end{aligned} \tag{2.39}$$

This simplification allows the forcing to be written as

$$\langle J(\rho,\psi)|_{\epsilon^2}\rangle = \frac{\mathrm{i}\omega}{\omega^2 - \sin^2\alpha\sin^2\theta}\left(\sin\alpha\cos\theta\frac{\partial}{\partial z} - \cos\alpha\frac{\partial}{\partial\xi}\right)J(Q,Q^*). \tag{2.40}$$

Then the vertical component, that is in $\hat{\boldsymbol{e}}_Z$, of the mean velocity is fully known by

(2.37),

$$\overline{W}_0 = \frac{\mathrm{i}\omega}{\omega^2 - \sin^2\alpha\sin^2\theta}\left(\sin\alpha\cos\theta\frac{\partial}{\partial z} - \cos\alpha\frac{\partial}{\partial\xi}\right)J(Q,Q^*). \tag{2.41}$$

The mean vertical velocity was determined independently of the mean horizontal flow; so we begin our investigation of the horizontal flow by first relating $\overline{U}$ with $\overline{V}$, which is most easily done with the Z-vorticity found by taking the cross product of (1.26a),

$$\frac{\partial}{\partial t}\Gamma + \frac{\partial}{\partial X}\left(\boldsymbol{u}\cdot\boldsymbol{\nabla}\overline{V}\right) - \frac{\partial}{\partial Y}\left(\boldsymbol{u}\cdot\boldsymbol{\nabla}\overline{U}\right) = 0, \tag{2.42}$$

where

$$\Gamma \equiv \frac{\partial}{\partial X}\overline{V} - \frac{\partial}{\partial Y}\overline{U} \tag{2.43}$$

is the vorticity in $\hat{\boldsymbol{e}}_Z$. The linear $\mathcal{O}(\epsilon)$ solution is

$$\Gamma = \Gamma_i(X,Y,Z) \tag{2.44}$$

independent of time. Note that the advective operators are kept in (ξ,ζ,z) since the spatial variation along the velocity vector is invariant in space. This allows us to write the time-averaged $\mathcal{O}(\epsilon^2)$ Z-vorticity as

$$\frac{\partial}{\partial X}\left\langle J(\overline{V},\psi)\big|_{\epsilon^2}\right\rangle - \frac{\partial}{\partial Y}\left\langle J(\overline{U},\psi)\big|_{\epsilon^2}\right\rangle = 0. \tag{2.45}$$

From the coordinate transformations of α and θ in figure 2-2, or more explicitly from (A.6a), we can show that the spatial derivatives in the original frame are

$$\frac{\partial}{\partial X} = \cos\alpha\cos\theta\frac{\partial}{\partial\xi} - \sin\alpha\frac{\partial}{\partial z}, \tag{2.46a}$$

$$\frac{\partial}{\partial Y} = \sin\theta\frac{\partial}{\partial\xi}, \tag{2.46b}$$

$$\frac{\partial}{\partial Z} = \sin\alpha\cos\theta\frac{\partial}{\partial\xi} + \cos\alpha\frac{\partial}{\partial z}. \tag{2.46c}$$

Applying (2.46) to (2.45), along with the general result (2.28),

$$\left(\cos\alpha\cos\theta\frac{\partial}{\partial\xi} - \sin\alpha\frac{\partial}{\partial z}\right)J(\overline{V},Q^*) - \left(\sin\theta\frac{\partial}{\partial\xi}\right)J(\overline{U},Q^*) + \text{c.c.} = 0. \tag{2.47}$$

The components $\overline{U}$ and $\overline{V}$ can be re-written by (2.35) so

$$\left(\cos\alpha\frac{\partial}{\partial\xi}-\sin\alpha\cos\theta\frac{\partial}{\partial z}\right)J(V,Q^*)-\sin\alpha\sin\theta\left(\frac{\partial}{\partial z}J(Q_z,Q^*)+\frac{\partial}{\partial\xi}J(Q_\xi,Q^*)\right)$$
$$+\text{c.c.}=0. \quad (2.48)$$

The same approach used previously in simplifying (2.31) shows that Jacobians in the second term can be reduced to

$$\frac{\partial}{\partial z}J(Q_z,Q^*)+\frac{\partial}{\partial\xi}J(Q_\xi,Q^*)+\text{c.c.}=J(\nabla^2Q,Q^*)+\text{c.c.} \quad (2.49)$$

In conjunction with (2.32) and (2.12b), the second term of (2.48) is identical to the first term. That is, Z-vorticity, which solely incorporates the horizontal velocity components does not reveal any information about the horizontal velocity. This finding suggests an arbitrariness associated with the steady-state mean flow. Lighthill [12, §5] astutely resolves this ambiguity in the context of addressing the initial-value problem; a similar approach is taken here. Upon time-averaging (2.43), and using the first-order result (2.44),

$$\frac{\partial}{\partial X}\overline{V}_0-\frac{\partial}{\partial Y}\overline{U}_0=\Gamma_i. \quad (2.50)$$

Since Γ_i is constant even in the unsteady development of the flow conditions up to leading order [12], it is entirely determined from the initial Z-vorticity distribution and approximately unchanged as the flow reaches steady-state. If we further call upon continuity,

$$\frac{\partial}{\partial X}\overline{U}_0+\frac{\partial}{\partial Y}\overline{V}_0=-\frac{\partial}{\partial Z}\overline{W}_0, \quad (2.51)$$

then each velocity component must satisfy Poisson's equation in every horizontal plane

$$\nabla_{\text{H}}^2\overline{U}_0=-\frac{\partial^2\overline{W}_0}{\partial Z\partial X}-\frac{\partial\Gamma_i}{\partial Y}, \quad (2.52)$$

$$\nabla_{\text{H}}^2\overline{V}_0=-\frac{\partial^2\overline{W}_0}{\partial Z\partial Y}+\frac{\partial\Gamma_i}{\partial X}, \quad (2.53)$$

where $\nabla_{\mathrm{H}}^2 = \partial^2/\partial X^2 + \partial^2/\partial Y^2$.

If we have knowledge of the initial vertical vorticity distribution, (2.52) and (2.53) can be integrated with the boundary conditions that the velocity normal to the slope is zero at the trace of the wave beam on the slope and that in the far-field the flow vanishes. Note that the mean flow vanishes outside of the overlap region since the Jacobians in (2.29) and (2.41) are zero in the far-field. The incoming and reflected wave beams satisfy the fully nonlinear equations so that there do not exist self-interactions to give rise to an induced mean flow.

2.3.3 Second-harmonics, $\mathcal{O}(\epsilon^2)$

Collecting now the $\mathcal{O}(\epsilon^2)$ terms in (2.4) which have time dependency $\mathrm{e}^{\mathrm{i}2\omega t}$, we have the following system of partial differential equations:

$$-\mathrm{i}2\omega V_2 - R_2 \sin\alpha \sin\theta = J(Q, V), \tag{2.54a}$$

$$-\mathrm{i}2\omega \left(Q_{2\xi\xi} + Q_{2zz}\right) + R_{2z} \sin\alpha \cos\theta - R_{2\xi} \cos\alpha = J(Q, Q_{\xi\xi} + Q_{zz}), \tag{2.54b}$$

$$-\mathrm{i}2\omega R_2 - Q_{2z} \sin\alpha \cos\theta + Q_{z\xi} \cos\alpha + V_2 \sin\alpha \sin\theta = J(Q, R). \tag{2.54c}$$

On the left-hand side are the forced second-harmonic terms and on the right-hand side are the interactions of the $\mathcal{O}(\epsilon)$ linear solution. The objective is to obtain an expression for Q_2 in terms of the incident beam from which the strength of the beam can be calculated.

To this end, (2.54a) and (2.54c) are combined to eliminate V_2 for R_2,

$$R_2 = \frac{\mathrm{i}2\omega \left(Q_{2z} \sin\alpha \cos\theta - Q_{2\xi} \cos\alpha\right) + J\left(Q, V \sin\alpha \sin\theta + \mathrm{i}2\omega R\right)}{4\omega^2 - \sin^2\alpha \sin^2\theta}. \tag{2.55}$$

The second term is fully known by the linear solution (2.12) and

$$\begin{aligned} R_2 =& \frac{\mathrm{i}2\omega \left(Q_{2z} \sin\alpha \cos\theta - Q_{2\xi} \cos\alpha\right)}{4\omega^2 - \sin^2\alpha \sin^2\theta} \\ &- \frac{\left(2\omega^2 + \sin^2\alpha \sin^2\theta\right) \left[J(Q, Q_z) \sin\alpha \cos\theta - J(Q, Q_\xi) \cos\alpha\right]}{\left(4\omega^2 - \sin^2\alpha \sin^2\theta\right) \left(\omega^2 - \sin^2\theta \sin^2\alpha\right)}. \end{aligned} \tag{2.56}$$

This result substituted into (2.54b) will yield an equation which involves only Q_2 and the linear solution Q. To do this, let us first evaluate the operation on R_2 in (2.54b),

$$\left(\sin\alpha\cos\theta\frac{\partial}{\partial z}-\cos\alpha\frac{\partial}{\partial\xi}\right)R_2 = \\ \frac{\mathrm{i}2\omega\left(Q_{2zz}\sin^2\alpha\cos^2\theta-2Q_{2z\xi}\sin\alpha\cos\alpha\cos\theta+Q_{2\xi\xi}\cos^2\alpha\right)}{4\omega^2-\sin^2\alpha\sin^2\theta} \\ -\frac{2\omega^2+\sin^2\alpha\sin^2\theta}{(4\omega^2-\sin^2\alpha\sin^2\theta)(\omega^2-\sin^2\theta\sin^2\alpha)}\Big\{[J(Q,Q_z)]_z\sin^2\alpha\cos^2\theta \\ -[J(Q,Q_z)]_\xi\sin\alpha\cos\alpha\cos\theta-[J(Q,Q_\xi)]_z\sin\alpha\cos\alpha\cos\theta+[J(Q,Q_\xi)]_\xi\cos^2\alpha\Big\}. \tag{2.57}$$

The terms in curly brackets can be reduced by expanding the Jacobians:

$$[J(Q,Q_z)]_z=\cancelto{0}{J(Q_z,Q_z)}+J(Q,Q_{zz}),\qquad [J(Q,Q_\xi)]_\xi=\cancelto{0}{J(Q_\xi,Q_\xi)}+J(Q,Q_{\xi\xi}),$$
$$[J(Q,Q_z)]_\xi=J(Q_\xi,Q_z)+J(Q,Q_{z\xi}),\qquad [J(Q,Q_\xi)]_z=J(Q_z,Q_\xi)+J(Q,Q_{\xi z}),$$

and noting that $[J(Q,Q_z)]_\xi+[J(Q,Q_\xi)]_z=2J(Q,Q_{z\xi})$. The second term on the right-hand side of (2.57) then becomes

$$-\frac{2\omega^2+\sin^2\alpha\sin^2\theta}{4\omega^2-\sin^2\alpha\sin^2\theta}J\left(Q,\frac{Q_{zz}\sin^2\alpha\cos^2\theta-2Q_{z\xi}\sin\alpha\cos\alpha\cos\theta+Q_{\xi\xi}\cos^2\alpha}{\omega^2-\sin^2\theta\sin^2\alpha}\right). \tag{2.58}$$

Recalling (2.13), the Jacobian collapses to the simple expression $J\left(Q,\nabla^2Q\right)$ and (2.57) is finally simplified to

$$\left(\sin\alpha\cos\theta\frac{\partial}{\partial z}-\cos\alpha\frac{\partial}{\partial\xi}\right)R_2 = \\ \frac{\mathrm{i}2\omega\left(Q_{2zz}\sin^2\alpha\cos^2\theta-2Q_{2z\xi}\sin\alpha\cos\alpha\cos\theta+Q_{2\xi\xi}\cos^2\alpha\right)}{4\omega^2-\sin^2\alpha\sin^2\theta} \\ -\frac{2\omega^2+\sin^2\alpha\sin^2\theta}{4\omega^2-\sin^2\alpha\sin^2\theta}J\left(Q,\nabla^2Q\right). \tag{2.59}$$

As promised, the partial differential equation for Q_2 is obtained by inserting (2.59) into (2.54b), followed by rearranging, to reveal

$$\boxed{\begin{aligned}&(4\omega^2-\sin^2\alpha\sin^2\theta-\cos^2\alpha)\frac{\partial^2 Q_2}{\partial\xi^2}\\&\qquad+2\sin\alpha\cos\alpha\cos\theta\frac{\partial^2 Q_2}{\partial z\partial\xi}+\left(4\omega^2-\sin^2\alpha\right)\frac{\partial^2 Q_2}{\partial z^2}=F_2(\xi,z),\end{aligned}} \tag{2.60}$$

where

$$F_2(\xi,z)=-\mathrm{i}3\omega J(\nabla^2 Q,Q). \tag{2.61}$$

Solving (2.60) is an involved exercise in mathematics, and the entirety of the next section is devoted to obtaining its solution. Until then, let us briefly inspect (2.60). We observe that the left-hand side is differentiated with respect to the spatial variables ξ and z, and the right-hand side is made up of the first-order forcing terms. Physically, this is another statement re-iterating the theme of the thesis; the first-order linear solution interacts with itself to provide a source for the generation of second-order wave beams of frequency 2ω.

2.4 Second-harmonic reflections

Because Q and Q_2 are finite in space, (2.60) can be removed of its explicit dependence on ξ by the Fourier transform

$$Q_2(\xi,z)=\int_{-\infty}^{\infty}\widehat{Q}_2(l;z)\mathrm{e}^{\mathrm{i}l\xi}\,\mathrm{d}l,\quad F_2(\xi,z)=\int_{-\infty}^{\infty}\widehat{F}_2(l;z)\mathrm{e}^{\mathrm{i}l\xi}\,\mathrm{d}l, \tag{2.62}$$

with the inverse transformation taking the form

$$\widehat{Q}_2(l;z)=\frac{1}{2\pi}\int_{-\infty}^{\infty}Q_2(\xi,z)\mathrm{e}^{-\mathrm{i}l\xi}\,\mathrm{d}\xi,\quad \widehat{F}_2(l;z)=\frac{1}{2\pi}\int_{-\infty}^{\infty}F_2(\xi,z)\mathrm{e}^{-\mathrm{i}l\xi}\,\mathrm{d}\xi. \tag{2.63}$$

Note that the integration is taken over l to correspond with the removal of ξ; this is not an arbitrary choice! The boundary condition (2.9) is specified along the slope, $z=0$, and is easily carried over to the spectral profiles $\widehat{Q}_2(l;z)$ and $\widehat{F}_2(l;z)$ granted

their z-dependence is explicit.

By substituting (2.62) into (2.60),

$$-l^2(4\omega^2 - \sin^2\alpha\sin^2\theta - \cos^2\alpha)\widehat{Q}_2(l;z) + \mathrm{i}2l\sin\alpha\cos\alpha\cos\theta\frac{\partial\widehat{Q}_2(l;z)}{\partial z} + \left(4\omega^2 - \sin^2\alpha\right)\frac{\partial^2\widehat{Q}_2(l;z)}{\partial z^2} = \widehat{F}_2(l;z), \quad (2.64)$$

we find the resulting equation to be susceptible to solutions common to linear ordinary differential equations, and in particular, the method of variation of parameters is quite suitable (see appendix B). The homogeneous solution is found by setting the forcing to zero and takes the form $\widehat{Q}_{2,\mathrm{h}} \sim \mathrm{e}^{\mathrm{i}\gamma}$ where γ is found to have multiple solutions from (2.64),

$$\gamma^{\pm} = l\sigma^{\pm}. \quad (2.65)$$

Here, $\sigma^{\pm}$, is exactly like the geometric factor $m^{\pm}$ in §2.3.1 for the linear reflection. As expected, it is also found with the same sequence of algebraic manipulations:

$$\sigma^{\pm} = -\cos\theta\frac{\sin\alpha\cos\alpha \mp r_2\sin\beta_2\cos\beta_2}{\sin^2\beta_2 - \sin^2\alpha}, \quad (2.66)$$

where

$$r_2 \equiv \sqrt{1 + \tan^2\theta\left(1 - \frac{\sin^2\alpha}{\sin^2\beta_2}\right)}. \quad (2.67)$$

The dispersion relation is implicit in the expression for $\sigma^{\pm}$ since $2\omega = \omega_2 = \sin\beta_2$. Note that for propagating second-harmonic waves, $\beta_2 < \pi/2$, so $\sin\beta_2 = 2\sin\beta < 1$ leads to the restriction

$$\beta < \pi/6. \quad (2.68)$$

Again, requiring $\sigma^{\pm}$ real ordains r_2 real as well, so

$$\sin^2\beta_2 > \sin^2\alpha\sin^2\theta. \quad (2.69)$$

However, this inequality is inconsequential since it readily follows from (2.16) and $\sin\beta_2 > \sin\beta$.

The homogeneous solution is a linear combination of the two quadratic solutions to $\gamma^{\pm}$,

$$\widehat{Q}_{2,\mathrm{h}}(l;z) = A^{+}(l)\mathrm{e}^{\mathrm{i}l\sigma^{+}z} + A^{-}(l)\mathrm{e}^{\mathrm{i}l\sigma^{-}z}. \tag{2.70}$$

The Wronskian, W, is calculated in preparing for engaging the variation of parameters,

$$W = \mathrm{i}2l\mathrm{e}^{\mathrm{i}l(\sigma^{+}+\sigma^{-})z}\left(r_2\frac{\cos\theta\sin\beta_2\cos\beta_2}{\sin^2\alpha-\sin^2\beta_2}\right). \tag{2.71}$$

Finally, the general solution to $\widehat{Q}_2$ is written as

$$\begin{aligned}\widehat{Q}_2(l;z) = &\left\{A^{+}(l) - \int_z^{\infty}\frac{\mathrm{i}\widehat{F}_2(l;\overline{z})\mathrm{e}^{-\mathrm{i}l\sigma^{+}\overline{z}}}{2lr_2\cos\theta\sin\beta_2\cos\beta_2}\,\mathrm{d}\overline{z}\right\}\mathrm{e}^{\mathrm{i}l\sigma^{+}z}\\ &+\left\{A^{-}(l) + \int_z^{\infty}\frac{\mathrm{i}\widehat{F}_2(l;\overline{z})\mathrm{e}^{-\mathrm{i}l\sigma^{-}\overline{z}}}{2lr_2\cos\theta\sin\beta_2\cos\beta_2}\,\mathrm{d}\overline{z}\right\}\mathrm{e}^{\mathrm{i}l\sigma^{-}z}.\end{aligned} \tag{2.72}$$

We are free choose the limits of integration as we like since $A^{\pm}(l)$ will pick up the remaining constant of integration. Therefore, it was decided to integrate from z to ∞ as a convenience allowing the far-field response to be represented without unnecessary clutter as

$$\widehat{Q}_2(l;z\to\infty) \to A^{+}(l)\mathrm{e}^{\mathrm{i}l\sigma^{+}z} + A^{-}(l)\mathrm{e}^{\mathrm{i}l\sigma^{-}z}. \tag{2.73}$$

Let us prematurely write the far-field streamfunction of the second-harmonic in real-space by inverse Fourier transform,

$$Q_2(\xi,z\to\infty) \to \int_{-\infty}^{\infty}\left\{A^{+}(l)\mathrm{e}^{\mathrm{i}l(\xi+\sigma^{+}z)} + A^{-}(l)\mathrm{e}^{\mathrm{i}l(\xi+\sigma^{-}z)}\right\}\,\mathrm{d}l \tag{2.74}$$

The expression (2.74) is especially useful for its vulnerability to investigation, in particular to our application of the radiation conditions which ensure causality. Comparison of (2.74) to the linear solution, (2.11) and (2.14), it is observed that the role of $\sigma^{\pm}$ in second-harmonic beams is played in the exact manner as $m^{\pm}$ in the primary-harmonic beams; that is, they define the direction of the cross-beam coordinate. For the sake of lucidity, we again revert back to the plane reflection ($\theta = 0$) for

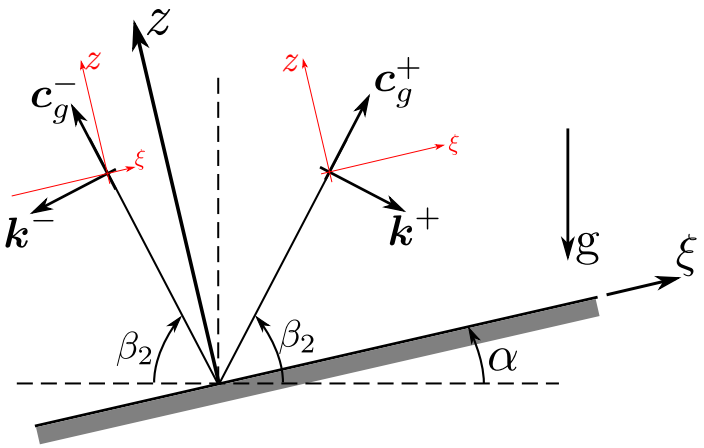

Figure 2-5: Possible radiated wave beams due to normal reflections. Energy is carried away from the reflection site, as indicated by group velocities, $\boldsymbol{c}_g^{\pm}$, which point outwards from the origin. The wavevectors, $\boldsymbol{k}^{\pm}$, are orthogonal with opposing vertical components to the group velocity. The radiation conditions may be applied to this scenario with the knowledge that only beams of wavenumbers with positive ξ-components are generated.

$\beta > \alpha$ in deference to the simplicity with which we can conjure visual aids for this configurations. The geometric factors in this case, $\sigma_0^{\pm} \equiv \sigma^{\pm}(\theta = 0)$, are

$$\sigma_0^+ = \cot(\alpha - \beta_2) < 0, \tag{2.75a}$$

$$\sigma_0^- = \cot(\alpha + \beta_2) > 0. \tag{2.75b}$$

The steps to achieve (2.75) are entirely analogous to those taken for acquiring (2.20) and have thus been omitted here.

There are two possible radiated wave beams in (2.74) as shown in figure 2-5. Both beams must have group velocity directed away from the reflection site and the associated wavevector is in accordance with (1.38) and (1.39). The designation of $\pm$ in figure 2-5 is ascertained by (2.75). Because σ_0^+ is negative, it relates to a wavevector with components of opposing sign, e.g, $\boldsymbol{k}^+$ is found in quadrant II or IV, with respect to the coordinates ξ and z. Similarly, $\boldsymbol{k}^-$ is expected in either quadrant I or III.

Recalling that the linear solution (2.11) is made up of only positive wavenumbers in ξ, that is $l > 0$, the forcing $F_2(\xi, z)$ in turn has contribution from $l > 0$ only. Formally, the Fourier transform $\widehat{F}_2(l; z)$ is written with infinite limits of integration

(2.63), but in examining the terms closely, it is seen that $\widehat{F}_2(l<0;z)=0$. This implies that radiated second-harmonics are generated with the restriction $l>0$, suggesting us to conclude that

$$A^-(l)=0. \tag{2.76}$$

The boundary condition (2.9) applied to second-harmonic beams,

$$\left.\frac{\partial Q_2}{\partial \xi}\right|_{z=0}=0, \tag{2.77}$$

leads to the transformed boundary condition

$$\widehat{Q}_2(l;z=0)=0. \tag{2.78}$$

In view of (2.76), this is easily carried against (2.72) and we find

$$A^+(l)=\int_0^\infty \frac{\mathrm{i}\widehat{F}_2(l;\overline{z})\left[\mathrm{e}^{-\mathrm{i}l\sigma^+\overline{z}}-\mathrm{e}^{-\mathrm{i}l\sigma^-\overline{z}}\right]}{2lr_2\cos\theta\sin\beta_2\cos\beta_2}\,\mathrm{d}\overline{z} \tag{2.79}$$

Finally, (2.74) is updated with our refined understanding to

$$Q_2(\xi,z\to\infty)\to\int_0^\infty A^+(l)\mathrm{e}^{\mathrm{i}l(\xi+\sigma^+z)}\,\mathrm{d}l. \tag{2.80}$$

The analysis of radiated second-harmonics is completed with an inquiry into the details of the source terms. Let us first expand the troublesome term in (2.61),

$$J(\nabla^2Q,Q)=\left(\nabla^2Q_\xi^{\mathrm{inc}}+\nabla^2Q_\xi^{\mathrm{ref}}\right)\left(Q_z^{\mathrm{inc}}+Q_z^{\mathrm{ref}}\right)-\left(\nabla^2Q_z^{\mathrm{inc}}+\nabla^2Q_z^{\mathrm{ref}}\right)\left(Q_\xi^{\mathrm{inc}}+Q_\xi^{\mathrm{ref}}\right), \tag{2.81}$$

and notice that it involves cross interactions between the incident and reflected beam, along with like interactions. Recall that in §1.6 it was found that a wave beam is an exact solution in the Boussinesq approximation with uniform density stratification, so we can justly expect like interactions to vanish. To verify, we calculate the terms

involving the incident beam interacting with itself,

$$\begin{aligned}
&\left(\nabla^2 Q_\xi^{\mathrm{inc}}\right) Q_z^{\mathrm{inc}} - \left(\nabla^2 Q_z^{\mathrm{inc}}\right) Q_\xi^{\mathrm{inc}} = \\
&\left(\int_0^\infty A(l) \Big\{ \overbrace{(\mathrm{i}l)}^{\partial/\partial\xi} \overbrace{\left[(\mathrm{i}l)^2 + (\mathrm{i}l m^{\mathrm{inc}})^2\right]}^{\nabla^2} \Big\} \mathrm{e}^{\mathrm{i}l\left(\xi + m^{\mathrm{inc}} z\right)} \, \mathrm{d}l \right) \left(\int_0^\infty A(l) \{ \overbrace{\mathrm{i}l m^{\mathrm{inc}}}^{\partial/\partial z} \} \mathrm{e}^{\mathrm{i}l\left(\xi + m^{\mathrm{inc}} z\right)} \, \mathrm{d}l \right) \\
&- \left(\int_0^\infty A(l) \Big\{ \underbrace{(\mathrm{i}l m^{\mathrm{inc}})}_{\partial/\partial z} \underbrace{\left[(\mathrm{i}l)^2 + (\mathrm{i}l m^{\mathrm{inc}})^2\right]}_{\nabla^2} \Big\} \mathrm{e}^{\mathrm{i}l\left(\xi + m^{\mathrm{inc}} z\right)} \, \mathrm{d}l \right) \left(\int_0^\infty A(l) \{ \underbrace{(\mathrm{i}l)}_{\partial/\partial\xi} \} \mathrm{e}^{\mathrm{i}l\left(\xi + m^{\mathrm{inc}} z\right)} \, \mathrm{d}l \right) .
\end{aligned} \tag{2.82}$$

In (2.82), the differential operations enacted on the incident beam (2.7), according to like terms from (2.81), are accentuated by curly brackets with the corresponding operation indicated by over/under braces. The factor m^{inc} can be pulled out from both terms to reveal that they are, in fact, completely identical; therefore, they entirely negate each other and again we are in a position to restate the essential physical insight that only cross interactions are relevant to the generation of second-harmonic internal wave beams. By the same token,

$$\left(\nabla^2 Q_\xi^{\mathrm{ref}}\right) Q_z^{\mathrm{ref}} - \left(\nabla^2 Q_z^{\mathrm{ref}}\right) Q_\xi^{\mathrm{ref}} = 0. \tag{2.83}$$

This physically significant result is illustrated in figure 2-6. Though beams do not interact with themselves, having the same frequency and angle of propagation, their cross interactions are important and are locally confined in the region in which the incident and reflected beam overlap. In the far-field, then, the second-harmonic beam is fully developed in agreement with (2.80).

The surviving cross terms of (2.81) can be resolved to

$$\begin{aligned}
J(\nabla^2 Q, Q) = &\left[\left(m^{\mathrm{ref}} - m^{\mathrm{inc}}\right) \left(1 + m^{\mathrm{ref}^2}\right) \right] \\
&\times \left\{ \int_0^\infty A(l) l^3 \mathrm{e}^{\mathrm{i}l\left(\xi + m^{\mathrm{ref}} z\right)} \, \mathrm{d}l \right\} \left\{ \int_0^\infty A(l) l \mathrm{e}^{\mathrm{i}l\left(\xi + m^{\mathrm{inc}} z\right)} \, \mathrm{d}l \right\}
\end{aligned}$$

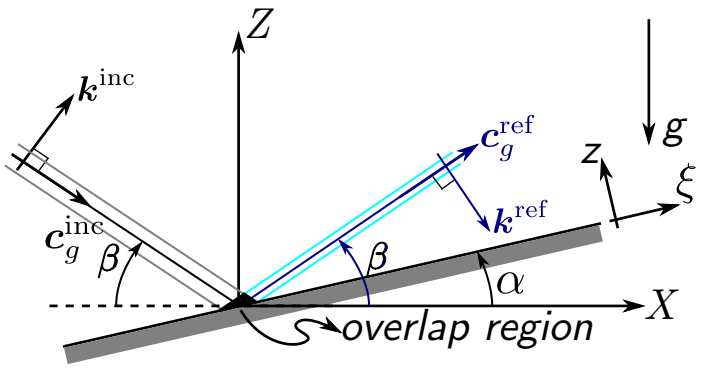

Figure 2-6: The linear solution predicts a primary reflection with the same angle to the horizontal as the incident beam. Interactions which give rise to second-harmonic beams are locally confined to the region of overlap. This region is indicated by dark shade.

$$+\left[\left(m^{\mathrm{inc}}-m^{\mathrm{ref}}\right)\left(1+{m^{\mathrm{inc}}}^2\right)\right] \times\left\{\int_0^\infty A(l)l^3\mathrm{e}^{\mathrm{i}l\left(\xi+m^{\mathrm{inc}}z\right)}\,\mathrm{d}l\right\}\left\{\int_0^\infty A(l)l\mathrm{e}^{\mathrm{i}l\left(\xi+m^{\mathrm{ref}}z\right)}\,\mathrm{d}l\right\}; \quad (2.84)$$

they involve multiplications of definite integrals which allows us to manipulate them to a more convenient form. For brevity, we will partially designate the integrand by $B(l;z)$ and specify its exact expression when germane. Presently, we will mould the integrals:

$$\left\{\int_0^\infty B_1(l_1;z)\mathrm{e}^{\mathrm{i}l_1\xi}\,\mathrm{d}l_1\right\}\left\{\int_0^\infty B_2(l_2;z)\mathrm{e}^{\mathrm{i}l_2\xi}\,\mathrm{d}l_2\right\}=\int_0^\infty\int_0^\infty B_1(l_1;z)B_2(l_2;z)\mathrm{e}^{\mathrm{i}\overbrace{(l_1+l_2)}^{l\equiv l_1+l_2}\xi}\,\mathrm{d}l_1\mathrm{d}l_2. \quad (2.85)$$

By defining $l\equiv l_1+l_2$ and eliminating the dummy variable l_2 in favour of l, and minding the restriction $l_2>0$, we can formally write $l_2=l-l_1>0$ so that $l>l_1$. The inner integral is over l_1 while l_2 is held constant, so $\mathrm{d}l=\mathrm{d}l_2$ and we can pull the exponential out of the inner integral so long that we are careful to restrict the limits

of integration from 0 to l in obedience to $l > l_1$. The right-hand side of (2.85) is then

$$\int_0^\infty \left\{ \int_0^l B_1(l_1; z) B_2(l - l_1; z) \, \mathrm{d}l_1 \right\} \mathrm{e}^{\mathrm{i}l\xi} \, \mathrm{d}l. \tag{2.86}$$

This is a noteworthy result since the term in brackets is the same form of the Fourier transform in (2.62). Not only have we simplified $F_2(\xi, z)$ but we also have the exact expression for $\widehat{F}_2(l; z)$ allowing us to evaluate $A^+(l)$ in (2.79) so that we have the radiated response (2.80). To be exact,

$$\begin{aligned} F_2(\xi, z) &= -\mathrm{i}3\omega J(\nabla^2 Q, Q) \\ &= \int_0^\infty -\mathrm{i}3\omega \Bigg\{ \left[\left(m^{\mathrm{ref}} - m^{\mathrm{inc}} \right) \left(1 + {m^{\mathrm{ref}}}^2 \right) \right] \int_0^l B_1(\bar{l}; z) B_2(l - \bar{l}; z) \, \mathrm{d}\bar{l} \\ &\qquad + \left[\left(m^{\mathrm{inc}} - m^{\mathrm{ref}} \right) \left(1 + {m^{\mathrm{inc}}}^2 \right) \right] \int_0^l B_3(\bar{l}; z) B_4(l - \bar{l}; z) \, \mathrm{d}\bar{l} \Bigg\} \mathrm{e}^{\mathrm{i}l\xi} \, \mathrm{d}l, \end{aligned} \tag{2.87}$$

where

$$\begin{aligned} B_1(\bar{l}; z) &= A(\bar{l}) \bar{l}^3 \mathrm{e}^{\mathrm{i}\bar{l} m^{\mathrm{ref}} z}, & B_2(\bar{l}; z) &= A(\bar{l}) \bar{l} \mathrm{e}^{\mathrm{i}\bar{l} m^{\mathrm{inc}} z}, \\ B_3(\bar{l}; z) &= A(\bar{l}) \bar{l}^3 \mathrm{e}^{\mathrm{i}\bar{l} m^{\mathrm{inc}} z}, & B_4(\bar{l}; z) &= A(\bar{l}) \bar{l} \mathrm{e}^{\mathrm{i}\bar{l} m^{\mathrm{ref}} z}, \end{aligned} \tag{2.88}$$

and finally,

$$\begin{aligned} \widehat{F}_2(l; z) = -\, \mathrm{i}3\omega \Bigg\{ & \left[\left(m^{\mathrm{ref}} - m^{\mathrm{inc}} \right) \left(1 + {m^{\mathrm{ref}}}^2 \right) \right] \int_0^l B_1(\bar{l}; z) B_2(l - \bar{l}; z) \, \mathrm{d}\bar{l} \\ & + \left[\left(m^{\mathrm{inc}} - m^{\mathrm{ref}} \right) \left(1 + {m^{\mathrm{inc}}}^2 \right) \right] \int_0^l B_3(\bar{l}; z) B_4(l - \bar{l}; z) \, \mathrm{d}\bar{l} \Bigg\}. \end{aligned} \tag{2.89}$$

Here, we have also made explicit that $\widehat{F}_2(l < 0; z) = 0$, reaffirming the role it played as part of the radiation conditions leading to (2.76). All variables of interest are now

expressed in terms of the incident beam, $A(l)$. In the next chapter, we prescribe $A(l)$ and illustrate the details of applying the preceding analysis in computation.

Chapter 3

Sample computations

The theoretical analysis of the previous chapter lead to the determination of the second-harmonic beam profile for reflection configurations given by the profile of the incident beam, the slope angle, the angle of propagation, and the degree of obliqueness. To gain more insight into the effects of obliqueness on energy transport, this chapter reports on the relevant quantities of chapter 2 over a range of parameters as computed for some sample incident beam profiles.

3.1 Beam profile

To ensure consistency of the assigned beam profile for all geometries, the incident beam is designated with regards to the cross-beam coordinate η,

$$Q^{\text{inc}}(\eta) = \int_0^\infty \widehat{Q}(\kappa) \mathrm{e}^{\mathrm{i}\kappa\eta} \, \mathrm{d}\kappa. \tag{3.1}$$

As a first example, we take the incoming beam to have Gaussian streamfunction,

$$\psi(\eta, t = 0) = \epsilon \mathrm{e}^{-2\eta^2}. \tag{3.2}$$

which serves to make for easy comparison with the plane reflections studied by Tabaei et al. [19].

In turn, the spectral density can be calculated from (1.51) and (2.5),

$$\mathrm{e}^{-2\eta^2} = \int_0^\infty \widehat{Q}^{\mathrm{inc}}(\kappa)\mathrm{e}^{\mathrm{i}\kappa\eta}\,\mathrm{d}\kappa + \int_0^\infty \widehat{Q}^{\mathrm{inc}^*}(\kappa)\mathrm{e}^{-\mathrm{i}\kappa\eta}\,\mathrm{d}\kappa. \tag{3.3}$$

Because the Fourier transform of a Gaussian is also Gaussian, the spectral amplitude is anticipated to take the form

$$\widehat{Q}^{\mathrm{inc}} = a\mathrm{e}^{-\kappa^2 b} \tag{3.4}$$

and the right-hand side of (3.3) can be combined to

$$\int_0^\infty a\mathrm{e}^{-\kappa^2 b}\mathrm{e}^{\mathrm{i}\kappa\eta}\,\mathrm{d}\kappa + \int_0^\infty a\mathrm{e}^{-\kappa^2 b}\mathrm{e}^{-\mathrm{i}\kappa\eta}\,\mathrm{d}\kappa = a\int_{-\infty}^\infty \mathrm{e}^{-b\kappa^2+\mathrm{i}\eta\kappa}\,\mathrm{d}\kappa, \tag{3.5}$$

by allowing the dummy variable in the second term to be substituted by its negative, $\kappa \to -\kappa$. Completing the square in the exponential,

$$a\int_{-\infty}^\infty \mathrm{e}^{-b\kappa^2+\mathrm{i}\eta\kappa}\,\mathrm{d}\kappa = a\mathrm{e}^{-\eta^2/4b}\int_{-\infty}^\infty \mathrm{e}^{-b(\kappa-\mathrm{i}\eta/2b)^2}\,\mathrm{d}\kappa, \tag{3.6}$$

and making the substitution

$$u = k - \mathrm{i}\eta/2b, \quad \mathrm{d}u = \mathrm{d}\kappa, \tag{3.7}$$

all that remains is a standard integral that can be evaluated analytically. Although we want to calculate the integral

$$I = \int_{-\infty}^\infty \mathrm{e}^{-bu^2}\,\mathrm{d}u, \tag{3.8}$$

it is easier to consider its square,

$$I^2 = \int_{-\infty}^\infty \mathrm{e}^{-bu^2}\,\mathrm{d}u\int_{-\infty}^\infty \mathrm{e}^{-bv^2}\,\mathrm{d}v = \int_{-\infty}^\infty\int_{-\infty}^\infty \mathrm{e}^{-b(u^2+v^2)}\,\mathrm{d}u\mathrm{d}v. \tag{3.9}$$

Introducing polar coordinates, $r^2 = u^2 + v^2$ and $\mathrm{d}u\mathrm{d}v = r\mathrm{d}r\mathrm{d}\theta$,

$$I^2 = \int_{\theta=0}^{2\pi} \int_{r=0}^{\infty} \mathrm{e}^{-br^2} r \, \mathrm{d}r\mathrm{d}\theta = 2\pi \int_{0}^{\infty} \left(\frac{1}{-2b} \right) \mathrm{e}^{-br^2} \, \mathrm{d}\left(-br^2\right) = \frac{\pi}{b}. \tag{3.10}$$

The parameters a and b for the specified Gaussian profile are found by substituting the result (3.10) and (3.6) into (3.3),

$$\mathrm{e}^{-2\eta^2} = a\sqrt{\frac{\pi}{b}}\mathrm{e}^{-\eta^2/4b}. \tag{3.11}$$

The expression for $\widehat{Q}^{\mathrm{inc}}$ according to (3.4) is then

$$\widehat{Q}^{\mathrm{inc}}(\kappa) = \sqrt{\frac{1}{8\pi}}\mathrm{e}^{-\kappa^2/8}. \tag{3.12}$$

Now that we have an expression to keep the assigned incident beam consistent with each variation of reflection geometry, it must be related to the alternate form used previously for analytical calculations,

$$Q^{\mathrm{inc}}(\xi, z) = \int_{0}^{\infty} A(l)\mathrm{e}^{\mathrm{i}l\left(\xi + m^{\mathrm{inc}} z\right)} \, \mathrm{d}l \tag{3.13}$$

This is done so by recognizing the cross-beam coordinate has the form

$$\eta = a\xi + bz \tag{3.14}$$

such that

$$a^2 + b^2 = 1. \tag{3.15}$$

The spatial coordinates in (3.13) can be converted into the cross-beam coordinate by determining the appropriate pre-factor,

$$\eta^{\mathrm{inc}} = \mathbb{C}\left(\xi + m^{\mathrm{inc}} z\right), \tag{3.16}$$

where $\mathbb{C}$ satisfies (3.15). It is then found that

$$\eta^{\text{inc}} = \sqrt{\frac{1}{1+m^{\text{inc}^2}}}\left(\xi + m^{\text{inc}} z\right). \tag{3.17}$$

Setting the two forms of incident beam, (3.1) and (3.13), equal to one another, we find that the integrated wavenumbers are linked by the pre-factor $\mathbb{C}$ as

$$\kappa = l\sqrt{1+m^{\text{inc}^2}}. \tag{3.18}$$

The relation between the integral expressions of the incident beam can then be consolidated with the matchings

$$A(l) = \sqrt{1+m^{\text{inc}^2}}\widehat{Q}^{\text{inc}}\left(l\sqrt{1+m^{\text{inc}^2}}\right), \tag{3.19a}$$

$$\widehat{Q}^{\text{inc}}(\kappa) = \frac{A\left(\kappa/\sqrt{1+m^{\text{inc}^2}}\right)}{\sqrt{1+m^{\text{inc}^2}}}. \tag{3.19b}$$

For the beam specified by (3.12),

$$A(l) = \sqrt{\frac{1+m^{\text{inc}^2}}{8\pi}}\mathrm{e}^{-l^2\left(1+m^{\text{inc}^2}\right)/8}, \tag{3.20}$$

where the consistency in beam profile for differing geometries is preserved by the factor m^{inc}.

Furthermore, we require the average energy flow rate in terms of $A(l)$. In the nondimensionalized Boussinesq approximation of §1.3, the average energy flow rate (1.59) is (see [19])

$$\mathcal{F} = 4\pi\cos\beta\int_0^\infty \kappa\left|\widehat{Q}(\kappa)\right|^2\,\mathrm{d}\kappa. \tag{3.21}$$

For the incident beam, we can directly apply (3.18) and (3.19a) to (3.21),

$$\mathcal{F}^{\text{inc}} = 4\pi\cos\beta\int_0^\infty l\left|A(l)\right|^2\,\mathrm{d}l. \tag{3.22a}$$

The foregoing calculations are preformed in an identical fashion with regards to the primary reflected beam (2.10) and the radiated second-harmonic (2.80) with the results

$$\mathcal{F}_1^{\text{ref}} = 4\pi \cos\beta \int_0^\infty l\,|A(l)|^2 \;\mathrm{d}l, \tag{3.22b}$$

$$\mathcal{F}_2^{\text{ref}} = 4\pi \cos\beta_2 \int_0^\infty l\,\left|A^+(l)\right|^2 \;\mathrm{d}l. \tag{3.22c}$$

3.2 Numerical results

3.2.1 Gaussian Profile

Ultimately, we desire the quantities in (3.22) for any given profile of the incident beam $A(l)$. The forcing $\widehat{F}_2(l;z)$ is numerically computed from (2.89) followed by $A^+(l)$ from (2.79). The average energy flow rates (3.22) are then found from performing the integrations. All integrals are carried out by the trapezoidal method. This process is then looped for various configurations of the slope angle α, the angle with which the incident beam propagates β, and the obliqueness of incidence θ. The computations are performed in `MATLAB` and the details of the code are included in appendix C.

The average energy flow rate of the second-harmonic beam relative to the incident beam is $\epsilon^2\overline{\mathcal{F}}_2$, where

$$\overline{\mathcal{F}}_2 = \frac{\mathcal{F}_2^{\text{ref}}}{\mathcal{F}^{\text{inc}}}. \tag{3.23}$$

The ratio above, for the incident beam (3.2), is reported in the following plots. Figure 3-1 shows curves varied over the slope angle α for selected angles of propagation β. Figure 3-1(a) is the case of a normal reflection ($\theta = 0°$). From before, $\beta < 30°$ for radiating second-harmonics. The most striking feature of these curves is the singularity at the critical angle, $\alpha = \beta$. Recall from §2.3.1 that for this particular incidence, the reflected beam is infinitesimally thin which subsequently causes $\widehat{F}_2(l;z)$ to become infinitely large along with the second-harmonic. As the curve approaches this critical angle from below, the intensity of the beam rapidly increases; similarly, it rapidly

diminishes just beyond criticality.

If we now take a high angle of obliqueness, $\theta = 75°$, as shown in figure 3-1(b), it is seen that the observations made in the instance of normal incidence have become more pronounced; the peak of the curve is more narrow and the energy flow rate beyond criticality drops off almost immediately. This latter effect is congruent with the restriction of beam generation addressed in appendix A. Viewed from the perspective of varying α for a fixed θ and β, the upper bound is set by the restriction (2.16). In a more general sense, the introduction of obliqueness reduces the strength of the generated second-harmonic. As an example, let us direct our attention towards the dashed-dot curve for $\beta = 25°$ for the particular slope angle $\alpha = 15°$. When $\theta = 0°$, the secondary beam is characterized by $\overline{\mathcal{F}}_2 \approx 425$; however, for $\theta = 75°$, one finds $\overline{\mathcal{F}}_2 \approx 75$. Although figure 3-1 compares the relative extremes of normal incidence to largely oblique incidence, similar plots with varying degrees of θ demonstrate a gradual development between the two plots presented here.

Figure 3-2 takes the view of varying the angle of propagation of the incident beam β for fixed slope α and obliqueness θ. Again, let us first look at the normal incidence, figure 3-2(a). It is immediately recognized that only one of the two curves contain the expected singularity at $\alpha = \beta$. Recall that the dispersion relation applied to radiating second-harmonic beams (2.68) requires

$$\beta < 30°. \tag{3.24}$$

Beyond this upper bound, the generated secondary beams are evanescent. Both curves satisfy the inequality and vanish as $\beta \to 30°$. Since the solid curve, $\alpha = 35°$, is unable to reach the critical angle $\alpha = \beta$ by the upper bound, there is no observed singularity. The dashed curve on the other hand, only gradually increases until it rapidly rises near the critical angle, beyond which it drops off as remarked earlier.

Now turning to the case of obliqueness $\theta = 45°$ in figure 3-2(b), we find again a reduction in beam intensity. This effect is most easily seen in the case of the solid curve for slope angle $\alpha = 45°$. For greater degrees of obliqueness, the solid curve is

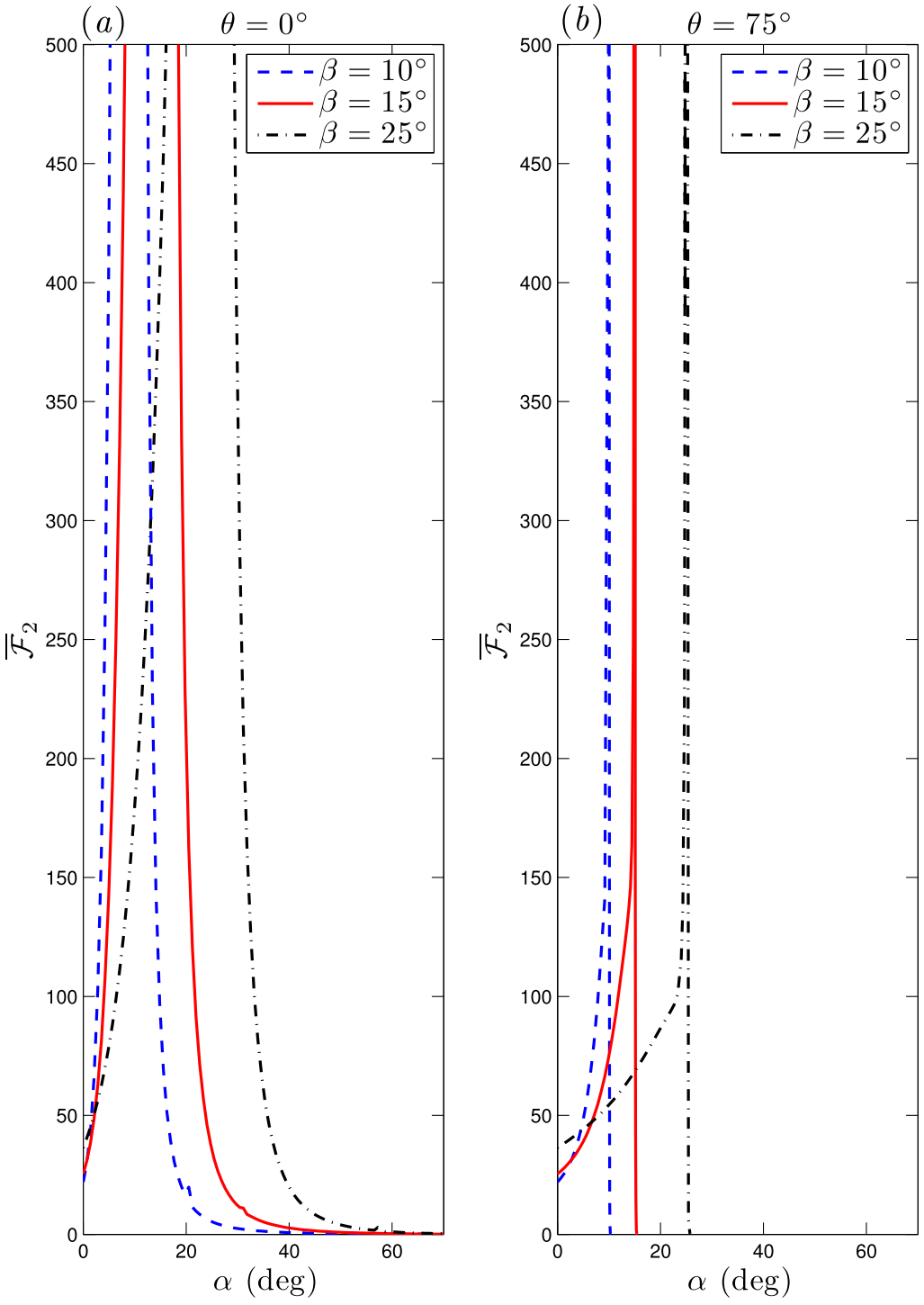

Figure 3-1: Normalized average energy flow rate of the second-harmonic beam for an incident beam of Gaussian profile, $e^{-2\eta^2}$. The curves are for fixed angles of propagation β as we vary the slope angle α. (a) For normal incidences, $\theta = 0°$. (b) For strongly oblique incidences, $\theta = 75°$ is considered. In both cases, the singularity at the critical angle $\alpha = \beta$ is observed.

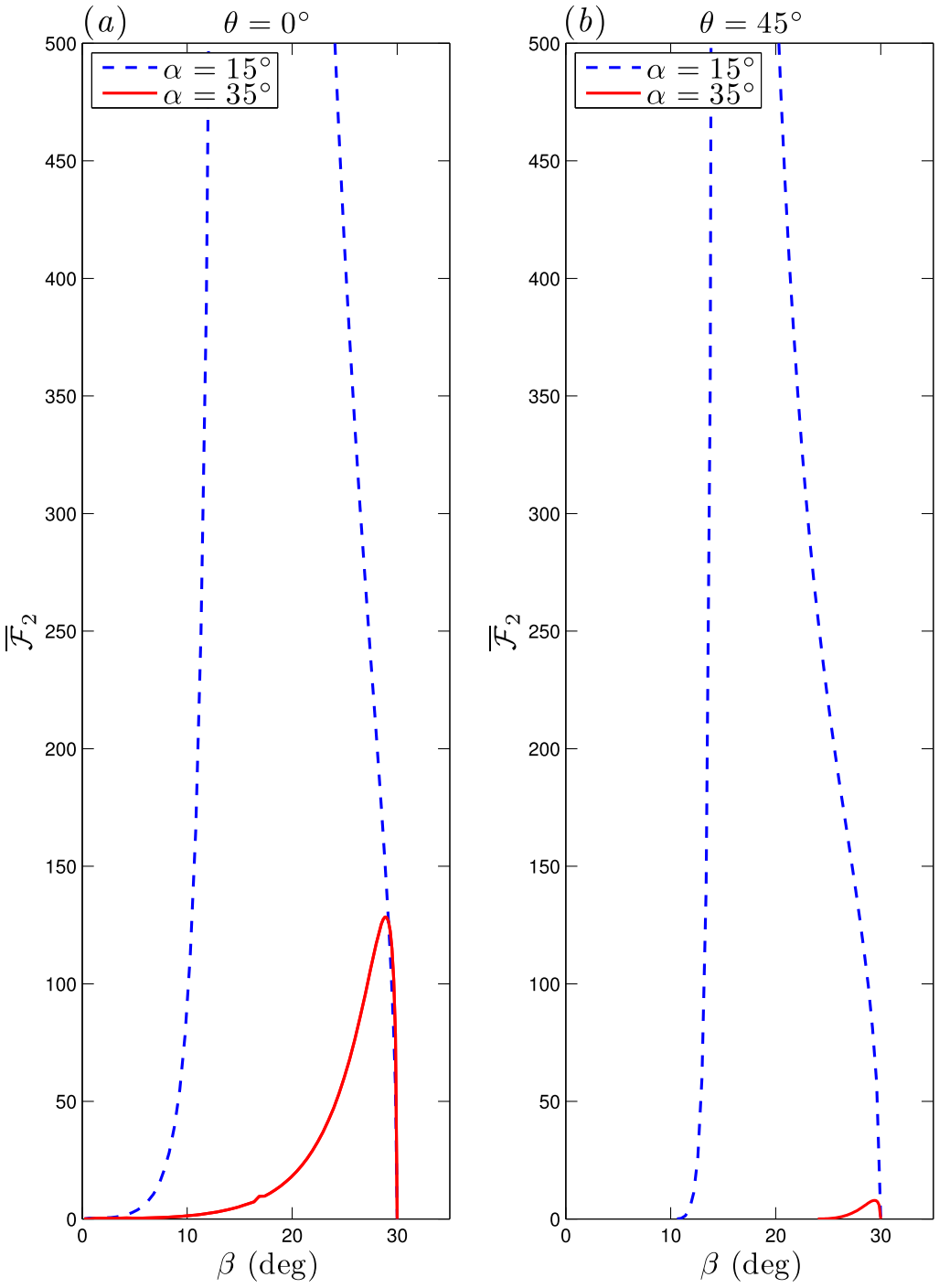

Figure 3-2: Normalized average energy flow rate of the second-harmonic beam for an incident beam of Gaussian profile. The curves are for fixed slope angles α as we vary angle of propagation β. (a) For normal incidences, $\theta = 0°$. (b) For oblique incidences, $\theta = 45°$ is considered. For greater degrees of obliqueness, the curve $\alpha = 35°$ is too small for clear observation.

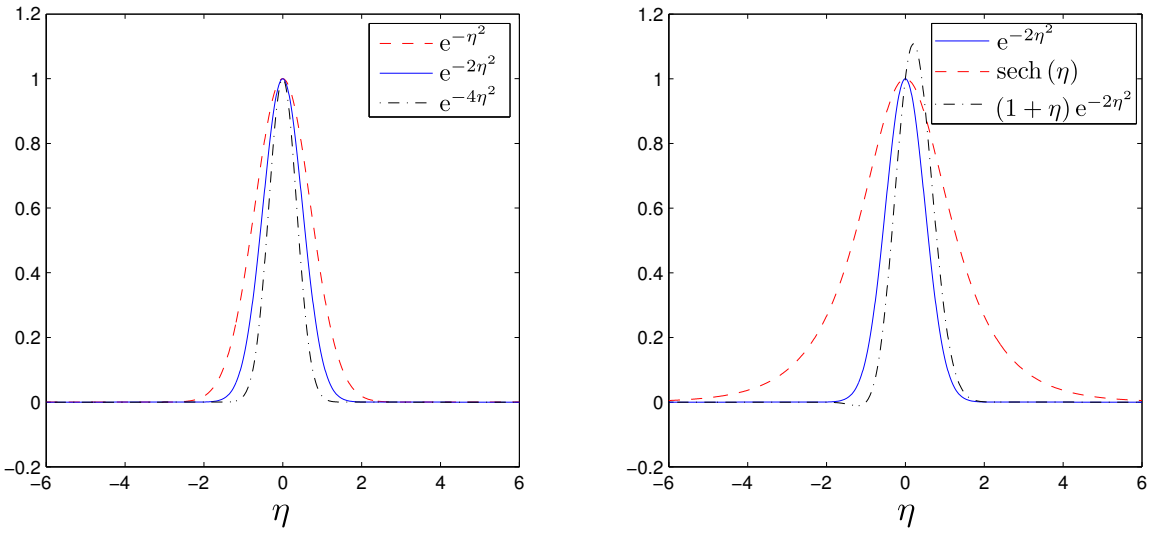

Figure 3-3: Incident streamfunction profile as a function of the cross-beam coordinate η. (a) Gaussian profile of various 'standard deviations'. (b) In the interest of variety, an alternate symmetric function, sech(η), and an asymmetric function, $(1+\eta)e^{-2\eta^2}$, are considered.

nearly zero. Note that both curves only take a value for $\overline{\mathcal{F}}_2$ when β passes a particular threshold. This is the restriction $\sin\beta > \sin\alpha \sin\theta$ discussed in appendix A. Carrying out the calculation explicitly, we find for the solid curve $\beta > 23.96°$; and for the dashed curve $\beta > 10.54°$. We also recognize that the dashed curve becomes more narrow when obliqueness is introduced, similar to the case described in figure 3-1.

The results of this section are in accordance with the previous investigation concerning the special case of normal incidences found by Tabaei et al. [19].

To investigate the effects of beam profile, we perform the same computations for various widths of Gaussian distributions as shown in figure 3-3(a). The results for the wider beam, $\epsilon e^{-\eta^2}$, are shown in figure 3-4, and for sharper beam, $\epsilon e^{-4\eta^2}$, in figure 3-5.

In general, one finds that for a sharper beam profile, the strength of the generated second-harmonic is greater. To understand this effect, let us return to the forcing of the second-harmonic beams as derived in §2.3.3. It was found that the overlap region confined to the reflection is the source of the weakly nonlinear beams according to (2.61), which claims the forcing is proportional to the spatial variations of the streamfunction, $F_2 \sim J(\nabla^2 Q, Q)$, rather than the overlap of streamfunction alone.

In fact, we can gain more insight by recalling the observation made during the

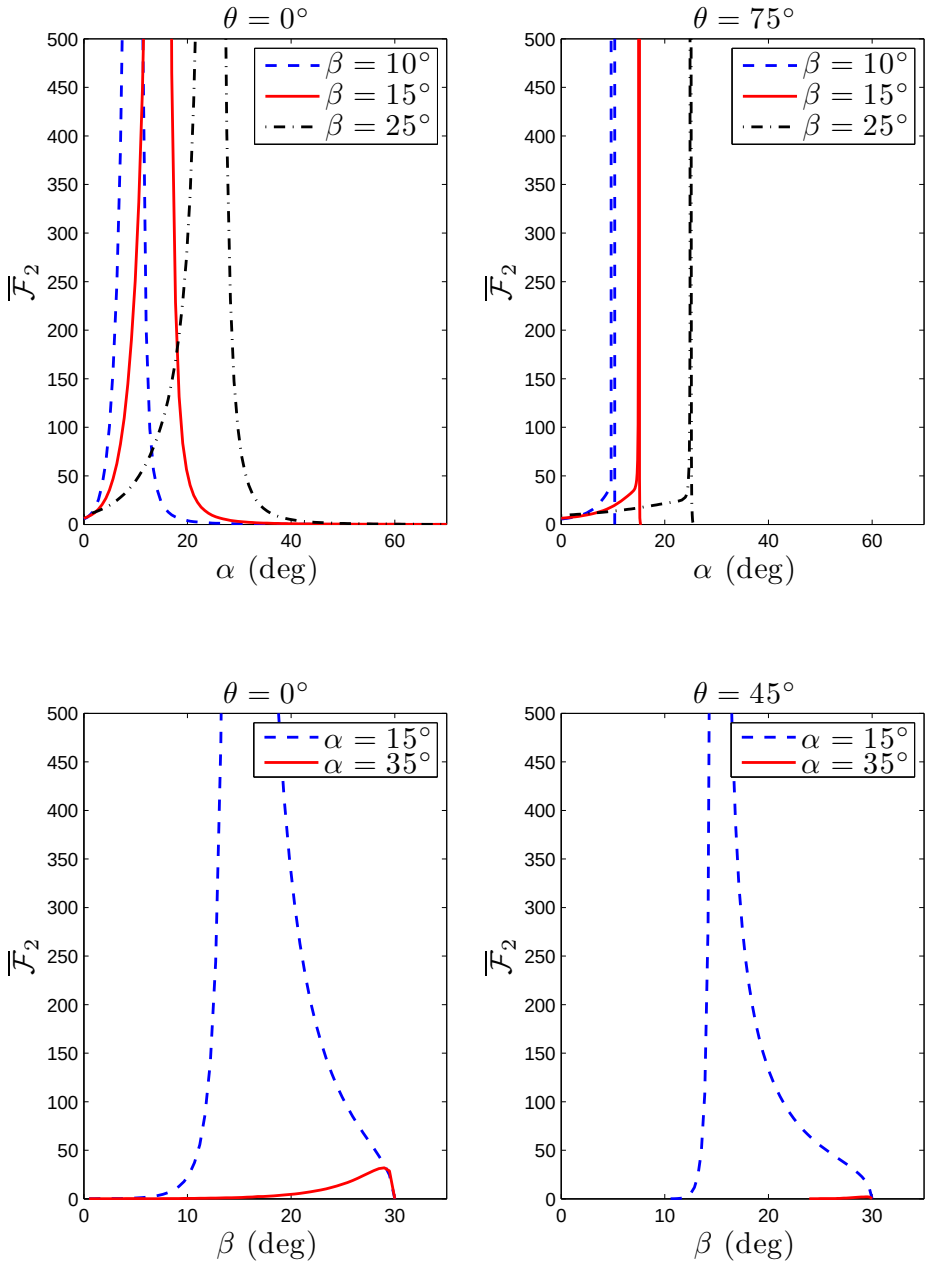

Figure 3-4: For an incoming beam of Gaussian profile $e^{-\eta^2}$, normalized average energy flow rates are calculated. In comparison to the results of figures 3-1 and 3-2, one finds that the wider profile produces a second-harmonic beam of weaker intensities.

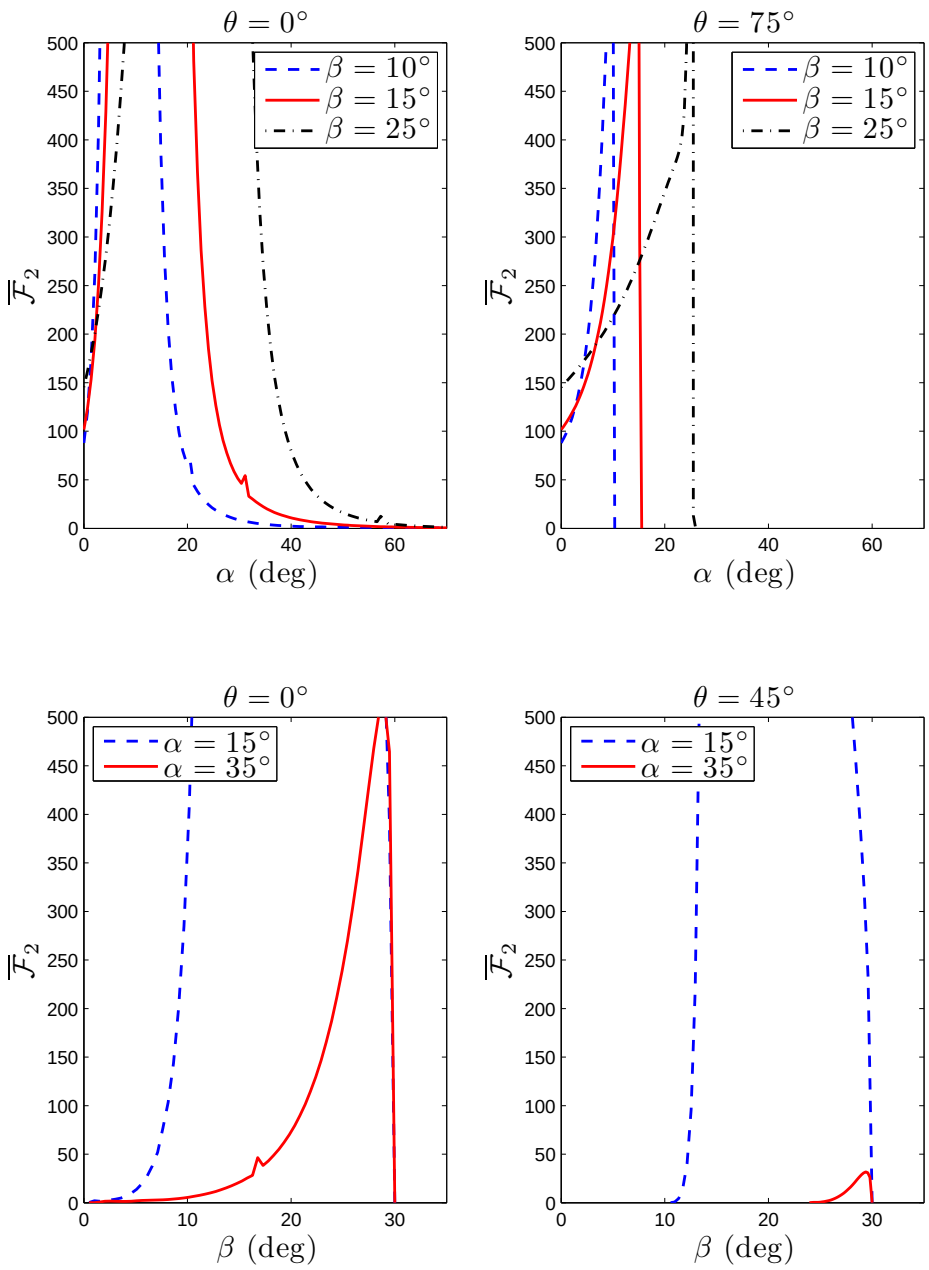

Figure 3-5: The average energy flow rates for a relatively sharp streamfunction profile of incident beam. As the spatial derivatives of the streamfunction are larger (sharper), the generated second-harmonic is of greater intensity. The effects of beam profile are described by the form of the quadratic forcing derived in chapter 2.

development of the governing equations §2.2 that the Jacobian of a quantity involving the streamfunction is the advective derivative of that quantity, i.e. $(\boldsymbol{u}\cdot\boldsymbol{\nabla})f = J(f,\psi)$. In addition to the recollection that the Laplacian of the streamfunction is the vorticity (in ζ here), it may be stated that the forcing is a manifestation of the interaction between the advected ζ-vorticity of the incident and primary reflected beam. By 'advected' vorticity, we mean the vorticity following a material fluid element in the Lagrangian sense.

There is one more observation to note, which is most clearly seen in figure 3-5 for the sharpest beam profile since the second-harmonics are greater in general. Whenever the angle $\alpha = \beta_2$, a small spike disrupts the smooth energy flow curves. Just as the linear solution becomes singular at the critical angle, $\alpha = \beta$, so does the second-order nonlinear solution at $\alpha = \beta_2$. This comes as no surprise in view of the analogous role that σ plays to m in §2.3. In the same way that m^{ref} blows up at the critical angle, σ^+ blows up at $\alpha = \beta_2$. However, note that the spike is much more narrow and even with a large increase in resolution in this region, the unbounded spike remains elusive.

3.2.2 Sech Profile

To introduce variety into our study, let us consider another beam profile defined by the streamfunction

$$\psi^{\text{inc}}(\eta, t=0) = \epsilon\,\text{sech}(\eta) = \epsilon\left\{\int_0^\infty \widehat{Q}(\kappa)\mathrm{e}^{\mathrm{i}\kappa\eta}\,\mathrm{d}\kappa + \int_0^\infty \widehat{Q}^*(\kappa)\mathrm{e}^{-\mathrm{i}\kappa\eta}\,\mathrm{d}\kappa\right\}. \tag{3.25}$$

The sech profile is plotted against the Gaussian taken earlier in figure 3-3(b). Notice that the sech function is much slower to converge, and based on the previous discussion we expect weaker second-harmonic beams to be generated.

In preparation of the computations to follow, we begin by reminding ourselves that the Fourier transform of the hyperbolic secant maintains its form, so we may use the same process as before in determining the the corresponding wavenumber profile

of the incident beam. In particular, we assume $\widehat{Q}(\kappa) = a\,\mathrm{sech}(b\kappa)$ and subsequently solve for a and b. The chosen function is real and even, allowing us to combine the integrals in (3.25) just as before when then Gaussian profile was taken. The Fourier transform is found from tables,

$$\int_{-\infty}^{\infty} \mathrm{sech}(b\kappa)\mathrm{e}^{\mathrm{i}\kappa\eta}\,\mathrm{d}\kappa = \frac{\pi}{b}\,\mathrm{sech}\left(\frac{\pi}{2b}\eta\right). \tag{3.26}$$

Omitting the redundancy of the algebra here, we only quote the result

$$\widehat{Q}(\kappa) = \frac{1}{2}\,\mathrm{sech}\left(\frac{\pi}{2}\kappa\right). \tag{3.27}$$

From (3.19),

$$A(l) = \frac{\sqrt{1+m^{\mathrm{inc}^2}}}{2}\,\mathrm{sech}\left(\frac{\pi}{2}l\sqrt{1+m^{\mathrm{inc}^2}}\right), \tag{3.28}$$

which is the expression most suitable for computations.

The results are shown in figure 3-6. The plots of the average energy flow rate resemble the case of the wide Gaussian considered in figure 3-4, although the generated second-harmonics are still weaker as expected by the smaller spatial derivatives.

3.2.3 Asymmetric profile

As a last example, we consider an asymmetric profile (see figure 3-3) made up of an odd and even part so that the incoming streamfunction defined in the cross-beam coordinate is

$$\psi^{\mathrm{inc}}(\eta, t=0) = \epsilon\left(\mathrm{e}^{-2\eta^2} + \eta\mathrm{e}^{-2\eta^2}\right) = \epsilon\left\{\int_0^{\infty}\widehat{Q}(\kappa)\mathrm{e}^{\mathrm{i}\kappa\eta}\,\mathrm{d}\kappa + \int_0^{\infty}\widehat{Q}^*(\kappa)\mathrm{e}^{-\mathrm{i}\kappa\eta}\,\mathrm{d}\kappa\right\}. \tag{3.29}$$

Making use of the general fact that the Fourier transform of the derivative of a function is

$$\int_{-\infty}^{\infty}\frac{df(x)}{dx}\mathrm{e}^{\mathrm{i}kx}\,\mathrm{d}x = \cancelto{0}{f(x)\mathrm{e}^{\mathrm{i}kx}\Big|_{-\infty}^{\infty}} - \mathrm{i}k\int_{-\infty}^{\infty} f(x)\mathrm{e}^{\mathrm{i}kx}\,\mathrm{d}x, \tag{3.30}$$

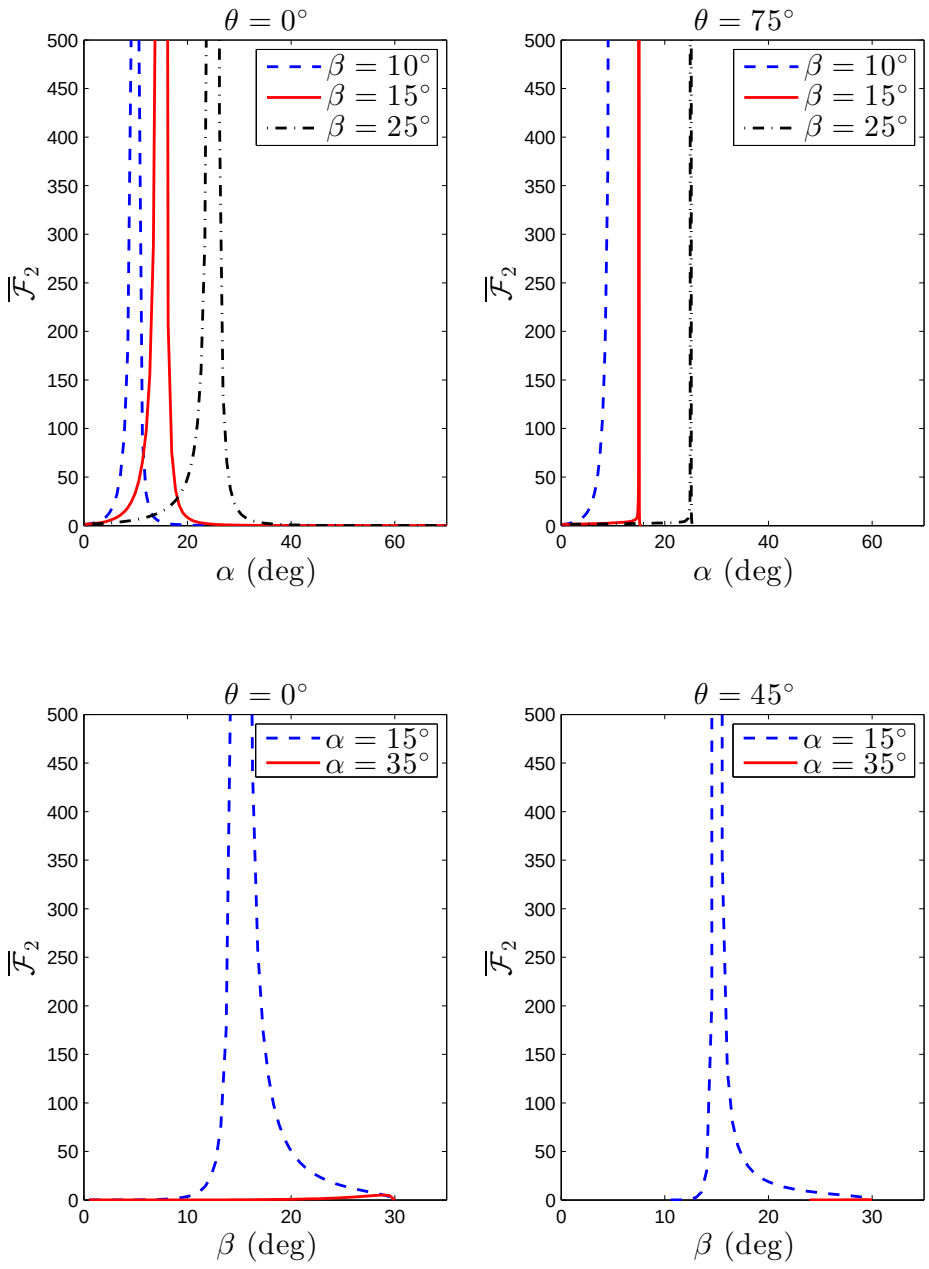

Figure 3-6: Normalized average energy flow rate for an incident beam of profile sech(η). The profile considered to generate this figure is the most slow to converge, resulting in weaker second-harmonic beams.

we anticipate the form of the spectral density,

$$\widehat{Q}^{\text{inc}}(\kappa) = a\mathrm{e}^{-\kappa^2 b} + \mathrm{i}\kappa a'\mathrm{e}^{-\kappa^2 b'}. \tag{3.31}$$

The first term is determined exactly as the purely Gaussian profile encountered earlier, so that $a = \sqrt{1/8\pi}$ and $b = 1/8$. The second term, placed into (3.29), can be simplified by expanding the oscillatory exponential in terms of sines and cosines. Only the even part remains, leaving

$$\eta\mathrm{e}^{-2\eta^2} = -2a' \int_0^\infty \kappa\mathrm{e}^{-\kappa^2 b'} \sin(\kappa\eta)\, \mathrm{d}\kappa. \tag{3.32}$$

The definite integral is looked up in the tables by Gradshteyn and Ryzhik [7, §3.952]. The anti-symmetric part of the spectral density is then

$$\eta\mathrm{e}^{-2\eta^2} = \frac{-a'\sqrt{\pi}}{2b'^{3/2}}\mathrm{e}^{-\eta^2/4b'}. \tag{3.33}$$

Solving for the remaining constants a' and b', (3.31) is

$$\widehat{Q}^{\text{inc}}(\kappa) = \sqrt{\frac{1}{8\pi}}\mathrm{e}^{-\kappa^2/8} - \mathrm{i}\frac{1}{8\sqrt{2\pi}}\kappa\mathrm{e}^{-\kappa^2/8}. \tag{3.34}$$

Subsequently (3.19) is applied and

$$A(l) = \left\{ \sqrt{\frac{1+m^{\text{inc}^2}}{8\pi}} - \mathrm{i}\frac{1+m^{\text{inc}^2}}{8\sqrt{2\pi}} l \right\} \mathrm{e}^{-l^2\left(1+m^{\text{inc}^2}\right)/8}. \tag{3.35}$$

The results are depicted in figure 3-7. In this case, spatial derivatives are only slightly larger than the for $\mathrm{e}^{-2\eta^2}$. Indeed, as expected the second-harmonic beam is stronger. The purpose, however, of this simulation is to look for any effects which may be associated with an incident beam having asymmetric beam profile. The plots in figure 3-7 suggest that there exist no such effects since all the characteristics of the curves can be accounted for by the discussion provided in the context of the

symmetric Gaussian cases in §3.2.1

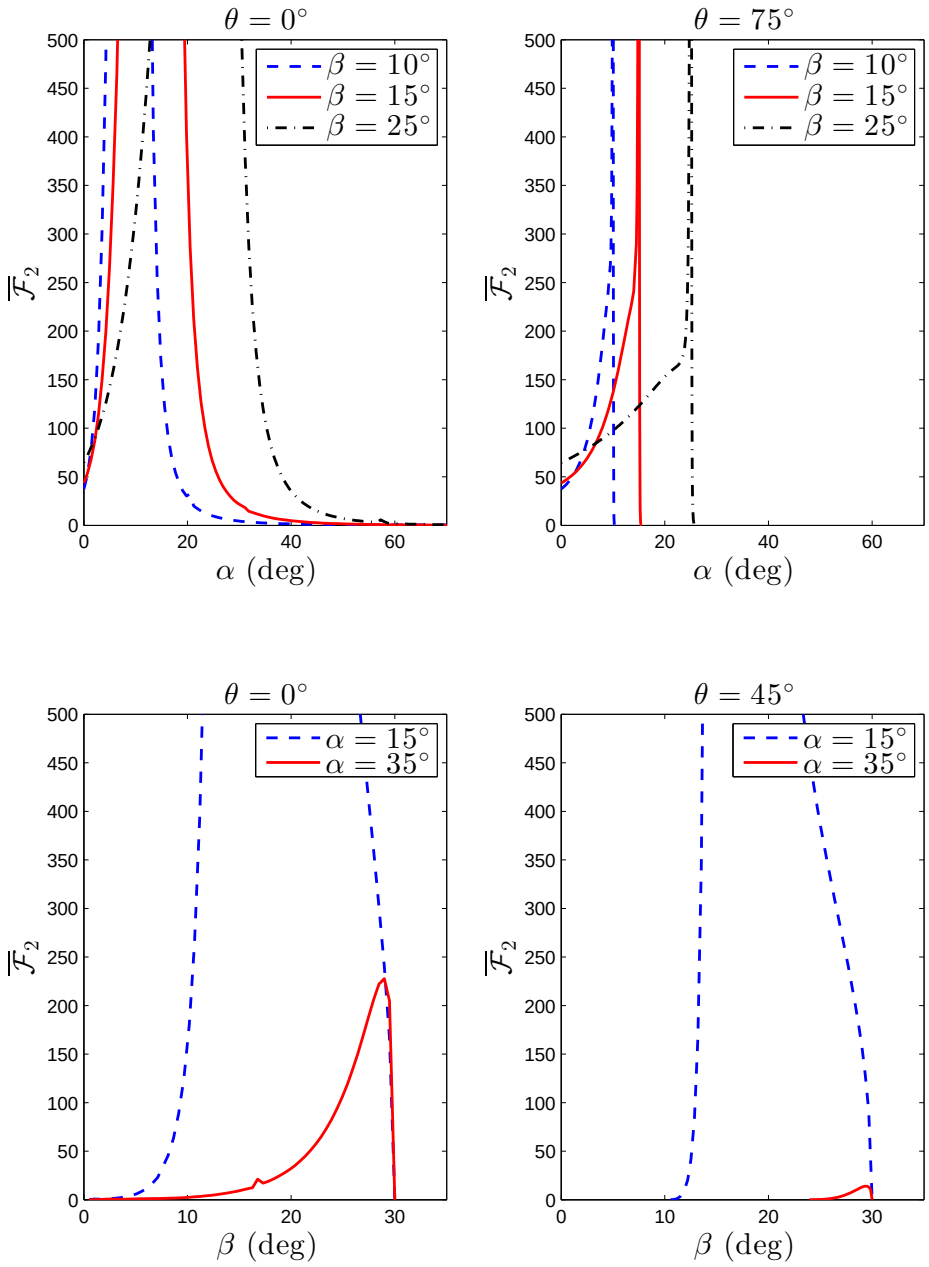

Figure 3-7: Investigating the effects of asymmetric streamfunction beam profile $(1+\eta)\,\mathrm{e}^{-2\eta^2}$. The value of the average energy flow rates follow the behaviour expected in light of the form of the second-harmonic forcing. However, there are no observed effects which are particular to an asymmetric profile.

Chapter 4

Concluding remarks

In this thesis, we have considered the reflections of internal gravity wave beams which are oblique relative to inclined topography. Viscous effects are ignored, and the beams are assumed to have amplitude sufficiently small so that weakly nonlinear theory is valid. Such a model can account for the generation of harmonic beams observed in earlier works [11].

Previously, Tabaei et al. [19] studied the special case for beams which are normally incident upon a slope. Our work is its direct extension and the approach here follows closely the theoretical development undertaken in the former. Furthermore, the special case of normal incidences serves as a check to our investigation.

First, defining the obliqueness of beams relative to a uniform incline, the governing equations within the confines of the inviscid, Boussinesq approximation were rewritten in a coordinate system suitable to the geometry at hand. Next, we allowed variables to take the form of weakly nonlinear expansions and solved the resulting linear equations to first and second order. By insisting the boundary condition—that the slope surface is impenetrable—applies for all time and everywhere on the slope, we found that the frequency, and hence the angle of propagation of the primary reflected beam (via dispersion relation) and the horizontal component of the wavenumber is conserved.

Moving on to the second-order solution, the induced mean flow was determined up to an arbitrary, initial spatial distribution of vertical vorticity. However, at steady-state the mean flow is locally confined and does not transport energy into the far-

field. The following time-dependent second-harmonic radiated wave beams were then calculated with the use of Fourier transform methods and applying the radiation conditions to ensure causality.

All relevant variables were determined in terms of the spectral density of the incident wave beam. To gain further insight, the average energy flow rate of the generated second-harmonic was numerically computed for various parameters and incident beam profiles. Although we only plotted the radiated energy carried by the nonlinear wave beam, our analytical calculations of chapter 2 give us the capability to determine the direction of beam propagation along with the exact profile of the primary and secondary reflected beams.

Some tangible remarks can be made on the basis of the numerics in chapter 3. In general, a wave beam incident upon a slope produces second-harmonic beams of maximum strength for in-plane scenarios. Relative obliqueness between the incoming wave beam and slope acts to decrease the intensity of generated nonlinear beams. In this sense, the results of normal reflections provide an upper bound of the weakly nonlinear effects. The effect of incident beam profile is contained within the degree of its spatial variations. Wave beams which are steeper (larger variation across the beam width) tend to generate second-harmonics of greater intensity, which conform to the source terms derived analytically. The computations are verified against Tabaei et al. [19] for uniformly incident beam of Gaussian spectral density.

At the critical angle, $\alpha = \beta$, inviscid theory predicts a singularity and it is suggested that a model which takes into account viscosity and finite amplitude effects will heal the unbounded steady-state solution.

As mentioned earlier in §2.1, collisions of wave beams also act as a source to yield additional wave beams. The linear solution assumes an inert process of superposition in which beams emerge undisrupted. A weakly nonlinear study was performed by Tabaei et al. [19] in which it was determined that the kinematics played a non-intuitive role in determining the direction of propagation with which the induced beams propagate due to plane collisions.

Future studies may be carried out which account for a relative obliqueness be-

tween two colliding beams such that they propagate in different vertical planes. The direction with which the induced beams propagate can be determined by applying the appropriate radiation conditions to wavevector kinematics which acquiesce to the form dictated by quadratic nonlinearities. Jiang and Marcus [8] presented the geometry of generated beams due to collisions for in-plane incidences; the results of which can be extended to the more general case of three-dimensional incidences.

Appendix A

Oblique Restriction

Requiring that the components of the wavevector are real, that is they indeed radiate, we found the restriction (2.16) reproduced here for convenience

$$\sin^2\beta > \sin^2\alpha \sin^2\theta. \tag{A.1}$$

To understand this inequality, the geometry of the rotated coordinate system (ξ, ζ, z) is compared against the the original frame (X, Y, Z) in the fully oblique case ($\theta = \pi/2$) with $\alpha > \beta$. For the beam $0 < \beta < \alpha$, it is impossible to satisfy (A.1).

The wavevector in each coordinate system can be written

$$(X, Y, Z): \qquad \boldsymbol{k} = k_X\hat{\boldsymbol{e}}_X + k_Y\hat{\boldsymbol{e}}_Y + k_Z\hat{\boldsymbol{e}}_Z, \tag{A.2a}$$

$$(\xi, \zeta, z): \qquad \boldsymbol{k} = k\hat{\boldsymbol{e}}_\xi + l\hat{\boldsymbol{e}}_\zeta + m\hat{\boldsymbol{e}}_z. \tag{A.2b}$$

However, the beams of interest are uniform in ζ so that

$$l = 0. \tag{A.3}$$

To match the two expressions of (A.2), we will explicitly perform the coordinate transformation as shown in figure A-1. The first step is a rotation by $-\alpha\hat{\boldsymbol{e}}_Y$ giving

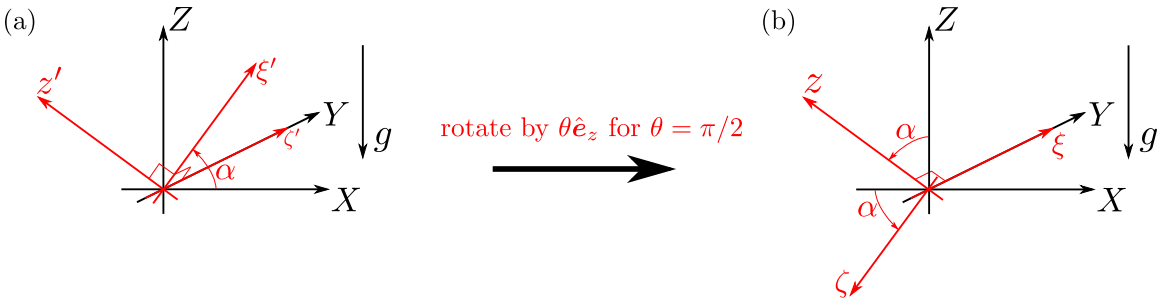

Figure A-1: The original reference frame is (X, Y, Z). (a) The rotation by α matches the slope, and (b) the rotation normal to the slope by θ accounts for obliqueness. The transformed coordinate system is (ξ, ζ, z). Here, the fully oblique case ($\theta = \pi/2$) is shown to highlight the possible discrepancy between uniformity in ζ and the dispersion relation.

us the intermediate frame (ξ', ζ', z):

$$\hat{\boldsymbol{e}}_{\xi'} = \cos\alpha\hat{\boldsymbol{e}}_X + \sin\alpha\hat{\boldsymbol{e}}_Y, \tag{A.4a}$$

$$\hat{\boldsymbol{e}}_{\zeta'} = \hat{\boldsymbol{e}}_Y, \tag{A.4b}$$

$$\hat{\boldsymbol{e}}_{z'} = -\sin\alpha\hat{\boldsymbol{e}}_X + \cos\alpha\hat{\boldsymbol{e}}_Z. \tag{A.4c}$$

The next rotation is in the direction normal to the slope, $\theta\hat{\boldsymbol{e}}_z$. The working reference frame in terms of the intermediate coordinates is

$$\hat{\boldsymbol{e}}_\xi = \cos\theta\hat{\boldsymbol{e}}_{\xi'} + \sin\theta\hat{\boldsymbol{e}}_{\zeta'}, \tag{A.5a}$$

$$\hat{\boldsymbol{e}}_\zeta = -\sin\theta\hat{\boldsymbol{e}}_{\xi'} + \cos\theta\hat{\boldsymbol{e}}_{\zeta'}, \tag{A.5b}$$

$$\hat{\boldsymbol{e}}_z = \hat{\boldsymbol{e}}_{z'}. \tag{A.5c}$$

and by (A.4) it can be written in the original frame as

$$\hat{\boldsymbol{e}}_\xi = \cos\theta\cos\alpha\hat{\boldsymbol{e}}_X + \cos\theta\sin\alpha\hat{\boldsymbol{e}}_Z + \sin\theta\hat{\boldsymbol{e}}_Y, \tag{A.6a}$$

$$\hat{\boldsymbol{e}}_\zeta = -\sin\theta\cos\alpha\hat{\boldsymbol{e}}_X + \cos\theta\hat{\boldsymbol{e}}_Y - \sin\theta\sin\alpha\hat{\boldsymbol{e}}_Z, \tag{A.6b}$$

$$\hat{\boldsymbol{e}}_z = \cos\alpha\hat{\boldsymbol{e}}_Z - \sin\alpha\hat{\boldsymbol{e}}_X. \tag{A.6c}$$

For the fully oblique case ($\theta = \pi/2$) along with the uniformity condition, $l = 0$,

the wavevector (A.2b) in (X, Y, Z) is

$$\boldsymbol{k} = -m \sin\alpha \hat{\boldsymbol{e}}_X + k\hat{\boldsymbol{e}}_Y + m\cos\alpha\hat{\boldsymbol{e}}_Z. \tag{A.7}$$

The condition $l = 0$ ensures uniformity in ζ and confines the wavevector to the ξz-plane. Such a wavevector must also satisfy the dispersion relation

$$\omega^2 = \frac{k_X^2 + k_Y^2}{k_X^2 + k_Y^2 + k_Z^2}. \tag{A.8}$$

As shown in §1.4, $\omega^2 = \sin^2\beta$ where β is the angle vertical to the wavevector (horizontal to the group velocity). This result, along with (A.7), can be substituted into (A.8) to determine the relationship between the wavevector components k (in ξ) and m (in z),

$$k^2 = m^2 \frac{\sin^2\beta - \sin^2\alpha}{\cos^2\beta}. \tag{A.9}$$

Now we may ask the significant question, "Do there exist radiating waves which satisfy the dispersion relation, and are simultaneously uniform along the ζ-axis?" Since radiating waves must have real wavenumbers, it is required that k and m are real. However, the result (A.9) suggests that if $\alpha > \beta$, either k or m is imaginary. This is exactly the restriction (A.1) we began to examine for the special case $\theta = \pi/2$.

Let us visualize this phenomena more closely by drawing the wavevector confined to the ξz-plane for $\beta > \alpha$ in which there is no violation of (A.1) against the situation $\alpha > \beta$ in which there is. Figure A-2 presents a side-by-side comparison. When $\beta > \alpha$, it is possible to generate a wave beam uniform in ζ for fully oblique incidences which still conform to the dispersion relation. However, if $\alpha > \beta$, then the wavevector cannot lie in the ξz-plane if it is to also satisfy the dispersion relation.

The restriction (A.1) is then interpreted as follows: it is not possible to generate a radiating beam of arbitrary obliqueness if $\alpha > \beta$. The degree of obliqueness is bounded by

$$\sin^2\theta < \frac{\sin^2\beta}{\sin^2\alpha}. \tag{A.10}$$

In fact, the preceding discourse can be treated more generally by taking the

(a) $\beta > \alpha$ (b) $\alpha > \beta$

Figure A-2: In the fully oblique incidence, $\theta = \pi/2$ and there exists conditions under which the generated wave beam will radiate. The geometry of the wavevector in blue is shown in accordance to the dispersion relation, $\omega = \sin\beta$. If it is also possible to construct the wavevector in the ξz-plane (shown in pink), then the corresponding wave beam will radiate. (a) $\beta > \alpha$ allows the wavevector in the ξz-plane to satisfy the dispersion relation. (b) $\alpha > \beta$ requires that the wavevector satisfy the dispersion relation lie *out* of the ξz-plane.

wavevector (A.7) for any θ,

$$\boldsymbol{k} = (k\cos\theta\cos\alpha - m\sin\alpha)\hat{\boldsymbol{e}}_X + (k\sin\theta)\hat{\boldsymbol{e}}_Y + (k\cos\theta\sin\alpha + m\cos\alpha)\hat{\boldsymbol{e}}_Z. \quad \text{(A.11)}$$

Then the dispersion relation (A.8) becomes

$$\omega^2 = \frac{(\cos\theta\cos\alpha - \frac{m}{k}\sin\alpha)^2 + \sin^2\theta}{1 + \left(\frac{m}{k}\right)^2}. \quad \text{(A.12)}$$

Because (A.1) is an inequality requiring β to exceed a particular threshold, we expect to find a minimum of $\sin^2\beta = \omega^2$ in (A.12). Taking derivatives with respect to the ratio m/k,

$$2\omega\frac{d\omega}{d(m/k)}^{0\ \text{(minimum)}} = \frac{-2\sin\alpha\left(\cos\theta\cos\alpha - \frac{m}{k}\sin\alpha\right)}{1 + \left(\frac{m}{k}\right)^2} - \frac{2\frac{m}{k}}{1 + \left(\frac{m}{k}\right)^2}\frac{\left(\cos\theta\cos\alpha - \frac{m}{k}\sin\alpha\right)^2 + \sin^2\theta}{1 + \left(\frac{m}{k}\right)^2}. \quad \text{(A.13)}$$

Removing common factors,

$$0 = \sin\alpha\left(\cos\theta\cos\alpha - \frac{m}{k}\sin\alpha\right)\left[1+\left(\frac{m}{k}\right)^2\right] + \frac{m}{k}\left[\left(\cos\theta\cos\alpha - \frac{m}{k}\sin\alpha\right)^2 + \sin^2\theta\right]. \tag{A.14}$$

Although the equation above appears to be cubic in m/k, the highest power terms cancel,

$$0 = \left(\cos\theta\cos\alpha - \frac{m}{k}\right)\overbrace{\left\{\left[1+\left(\frac{m}{k}\right)^2\right]\sin\alpha + \frac{m}{k}\left(\cos\theta\cos\alpha - \frac{m}{k}\sin\alpha\right)\right\}}^{\sin\alpha + \frac{m}{k}\cos\theta\cos\alpha} + \frac{m}{k}\sin^2\theta. \tag{A.15}$$

Finally, the quadratic in m/k is

$$\left(\frac{m}{k}\right)^2(-\sin\alpha\cos\alpha\cos\theta) + \left(\frac{m}{k}\right)\overbrace{(\cos^2\theta\cos^2\alpha - \sin^2\alpha + \sin^2\theta)}^{\cos^2\alpha - \cos^2\theta\sin^2\alpha} + \cos\theta\cos\alpha\sin\alpha = 0, \tag{A.16}$$

where the coefficients of the second term were rewritten by the identity $\cos^2\alpha = 1 - \sin^2\alpha$. The two roots are

$$\frac{m}{k} = \begin{cases} -\cos\theta\sin\alpha/\cos\alpha & (+) \\ \cos\alpha/\sin\alpha\cos\theta & (-) \end{cases} \tag{A.17}$$

where the result $(+)$ is meaningless since the ratio m/k must be positive. Taking the root $(-)$ for m/k into (A.12) yields

$$\omega^2\big|_{\min} = \sin^2\alpha\sin^2\theta. \tag{A.18}$$

This result re-discovers (A.1) by determination of ω from the dispersion relation in terms of the ratio of wavevector components, m/k, in the ξz-plane. Again, the significance of this finding is that (A.1) ensures that the wave beams have wavevector lying in the ξz-plane so that they are uniform in ζ and simultaneously satisfy the dispersion relation.

Although such a lengthy discussion of a side topic is not necessary, we do not

believe it is unwarranted. The restriction found in §2.3.1 has no counterpart in the case of normal incidences ($\theta = 0$) and cannot be interpreted so easily by inspection. It is solely the characteristic of a three-dimensional reflection. Thus, the inequality was given a thorough examination; first, with the use of visual aides, and second, with a more rigorous mathematical interrogation.

Appendix B

Variation of parameters

If the homogeneous solution to a linear differential question is known, then the corresponding nonhomogeneous solution can be determined by the method of variation of parameters. The only restriction is that the forcing—the inhomogeneity—is continuous. The following discussion has been adopted from Kreyszig [9, §2.10] and Tenenbaum and Pollard [20, §22].

Consider the second-order linear ordinary differential equation

$$f_2(x)y'' + f_1(x)y' + f_0(x)y = r(x), \tag{B.1}$$

where prime ($'$) denotes differentiation with respect to the independent variable x and, in general, the coefficients are also functions of x. The inhomogeneity is due to the function on the right-hand side, $r(x)$. If the homogeneous solution is known,

$$y_\mathrm{h} = c_1 y_1 + c_2 y_2, \tag{B.2}$$

which satisfies (B.1) for $r(x) = 0$, then the particular solution is assumed to take the form

$$y_\mathrm{p} = u_1(x)y_1(x) + u_2(x)y_2(x). \tag{B.3}$$

Taking first and second derivatives of (B.3) and substituting back into (B.1), we find

after some rearranging,

$$\cancelto{0}{u_1(f_2y_1'' + f_1y_1' + f_0y_1)} + \cancelto{0}{u_2(f_2y_2'' + f_1y_2' + f_0y_2)} + f_2\left[(u_1''y_1 + u_2''y_2) + 2(u_1'y_1' + u_2'y_2')\right] + f_1\left(u_1'y_1 + u_2'y_2\right) = r. \tag{B.4}$$

The first two terms vanish since the homogeneous solutions (B.2) satisfy (B.1) for $r = 0$. Thus far, we have only one equation, (B.4), to solve for two unknowns, u_1 and u_2. This enables us to freely impose a second restriction at our convenience. Taking a moment to examine the remaining terms in (B.4), it becomes clear that the terms in square brackets, coefficients to f_2, can be rewritten to show some semblance to the terms multiplied with f_1,

$$f_2\left[\frac{d}{dx}\left(u_1'y_1 + u_2'y_2\right) + \left(u_1'y_1' + u_2'y_2'\right)\right] + f_1\left(u_1'y_1 + u_2'y_2\right) = r. \tag{B.5}$$

In view of (B.5), it is apparent that the best choice of this restriction is

$$u_1'y_1 + u_2'y_2 = 0, \tag{B.6a}$$

so that

$$u_1'y_1' + u_2'y_2' = \frac{r}{f_2}. \tag{B.6b}$$

This system of algebraic equations can be solved for derivatives of u,

$$u_1' = -\frac{-y_2r}{Wf_2}, \qquad u_2' = \frac{y_1r}{Wf_2}, \tag{B.7}$$

where $W \equiv y_1y_2' - y_2y_1'$ is known as the Wronskian. Integrating (B.7), the particular solution is known and the general solution is the sum of y_h and y_p,

$$\boxed{y = \left(c_1 - \int \frac{y_2r}{Wf_2}\,\mathrm{d}x\right)y_1 + \left(c_2 + \int \frac{y_1r}{Wf_2}\,\mathrm{d}x\right)y_2.} \tag{B.8}$$

Notice that the limits of integration have been left blank. They are determined, along with the constants c_1 and c_2, upon application of boundary conditions unspecified

here. As a final remark, this second-order analysis can be readily extended to an n^{th}-order system [20].

Appendix C

M-Code

The core MATLAB code used to produce the results in chapter 3 is printed here. The primary script is contained in `main.m` in which the user selects the configuration over a range of slope angles, α, and propagation angles of incident beam, β. The details of the spectral density of the incident beam are held in `beamA.m` which takes the wavenumber, l, and geometric factor, m^{inc}, as input. Finally, the convolution-type integral in (2.89) is computed by `mconv2.m`.

Since both upper limits in the double integral are ∞, particular care must be taken in choosing the ranges of l and z. All quantities have been normalized in the early stages so that they are of order one. As a verification, the script `main.m` plots $A^{+}(l)$ over every $\overline{\mathcal{F}}_2$ computation and the user is to confirm its convergence.

main.m

```
clc, clear all, close all
% main.m: Main script which returns average energy flow rate of second-
%         harmonic for selected configurations
% input:
%     a = alpha, the slope angle
%     B = beta, the incident beam angle of propagation
%     th = theta, the angle of obliqueness
% output:
%     FL21 = normalized average energy flow rate of second-harmonic beam


    % slope angle
% a = 35*pi/180;
```

```
a = linspace(0,70,100)*pi/180;

    % angle of propagation
% B = linspace(16.4,17,30)*pi/180;
B = 15*pi/180;

    % relative obliqueness
th = 0*(pi/180);

    % limits of integration (these must be verified for convergence by
        % conferring with plots of A_p)
l = linspace(0.001,15,450); % range of wavenumbers
z = linspace(0,4,length(l)); % range of coordinate normal to slope

FL21 = NaN(length(a),length(B)); % place-holder for output

% Double for-loop over range of a and B
for ai = 1:length(a)
for bi = 1:length(B)

    % preliminary calculations for chosen parameters:
% trigonometry
sth = sin(th); cth = cos(th); tth = tan(th);
sB = sin(B(bi)); cB = cos(B(bi));
sa = sin(a(ai)); ca = cos(a(ai));
w = sB;
B2 = asin(2*sB);
sB2 = sin(B2); cB2 = cos(B2);

% geometric factors
r = sqrt(1 + tth^2*(sB^2-sa^2)/sB^2);
m_inc = cth*(r*cB*sB - sa*ca)/(sB^2-sa^2);
m_refl = -cth*(r*cB*sB + sa*ca)/(sB^2-sa^2);
r2 = sqrt(1+tth^2*(sB2^2-sa^2)/sB2^2);
si_p = -cth*(r2*cB2*sB2 + sa*ca)/(sB2^2-sa^2);
si_m = cth*(r2*cB2*sB2 - sa*ca)/(sB2^2-sa^2);

    % incident beam defined in function beamA.m
A = beamA(l,m_inc);

   % calculating the second-harmonic spectral forcing F2(l,z)
F2 = zeros(length(l),length(z));
fprintf('time to calculate F2:\n');
tic
   % define functions to be passed through convolution-type integrals
b1 = @(l) beamA(l,m_inc).*l.^3.*exp(1i*l.*m_refl.*z);
b2 = @(l) beamA(l,m_inc).*l.*exp(1i*l.*m_inc.*z);
b3 = @(l) beamA(l,m_inc).*l.^3.*exp(1i*l.*m_inc.*z);
b4 = @(l) beamA(l,m_inc).*l.*exp(1i*l.*m_refl.*z);
   % for every wavenumber, l, we integrate the forcing expressions over z
for k = 1:length(l)
    I1 = mconv2(b1,b2,0,l(k),length(z));
    I2 = mconv2(b3,b4,0,l(k),length(z));
    F2(k,:) = -1i*3*w*(((m_refl-m_inc)*(1+m_refl^2))*I1 +...
```

```
        (m_inc-m_refl)*(1+m_inc^2)*I2);
end
toc

   % calculate A_p(l), the second-harmonic streamfuntion in wavenumber domain
A_p = zeros(1,length(l));
for k = 1:length(l)
    integrand = F2(k,:).*(exp(-1i*l(k)*si_p.*z)-exp(-1i*l(k)*si_m.*z));
    I1 = trapz(z,integrand);
    A_p(k) = 1i./(l(k)*r2*cos(th)*sin(2*B2))*I1;
end

   % calculating energy fluxes:
% average energy of incident wave beam, FL_inc
integrand = l.*abs(A).^2;
I = trapz(l,integrand);
FL_inc = 4*pi*cos(B(bi))*I;

% average energy flow rate of secondary reflected wave beam, FL2
integrand = l.*abs(A_p).^2;
I = trapz(l,integrand);
FL2 = 4*pi*cos(B2)*I;

% normalized average energy flow rate of secondary reflected beam, FL21
FL21(ai,bi) = FL2/FL_inc;
fprintf('The ratio F21 = %0.5g:\n',FL21);

   % check the curve A_p to ensure it converges for the range of l and behaves
     % consistently for range of z
figure(4)
hold on
plot(l,real(A_p))
plot(l,imag(A_p),'--r')
legend('real','imaginary','Location','SouthEast')
title('A_+(l)')
xlabel('l')
ylabel('A_+')

end %closes loop over a
end %closes loop over B

save('B15_th0.mat','a','B','FL21') % data saved and plotted separately
```

beamA.m

```
function [A] = beamA(l,m)
%beamA
% input:
%     l = wavenumber
%     m = geometric factor of incoming wave, m_inc
%
% output:
```

```
%     A = beam profile in wavenumber domain

A = zeros(1,length(l));
for i = 1:length(l)
%     % Gaussian profile
%     A(i) = sqrt((1+m^2)/(4*pi))*exp(-l(i).^2*(1+m^2)/4); % 'wide'
%     A(i) = sqrt((1+m^2)/(8*pi))*exp(-l(i).^2*(1+m^2)/8); % 'standard'
%     A(i) = sqrt((1+m^2)/(16*pi))*exp(-l(i).^2*(1+m^2)/16); % 'narrow'

%     % Hybperbolic secant profile
%     A(i) = sqrt(1+m^2)/2*sech(l(i)*pi/2*sqrt(1+m^2));
%     % sech2
%     A(i) = sqrt(1+m^2)/4*sech(l(i)*pi/4*sqrt(1+m^2));

%     % Asymmetric profile
    A(i) = (sqrt((1+m^2)/(8*pi)) - 1i/(8*sqrt(2*pi))*(1+m^2).*l(i))...
    .*exp(-l(i).^2*(1+m^2)/8);
end
end
```

mconv2.m

```
function [S] = mconv2(A1,A2,a,b,lt)
% mconv2: Modified Convolution
%   calculates a modified convolution, which is the convolution integral
%   but with the limits a to b
%   S = mconv(A1,A2,a,b,lt)
% input:
%     A1 = function of the dummy variable, (l)
%     A2 = function of the 'reduced' dummy variable, (b-l)
%     a = lower bound of integration
%     b = upper bound of integration
%     lt = vector length of the spatial variable z (held constant); used
%          for pre-allocation
%
% output:
%     S = the summation (integral) of the modified convolution, which will
%         be a function of space (z)

% calculate the integrand of the convolution
n1 = linspace(a,b,150);
integrand = zeros(length(n1),lt); %preallocate
for i = 1:length(n1)
    integrand(i,:) = A1(n1(i)).*A2(b-n1(i));
end

% the integrand is a matrix (l,z), where we want to integrate over l
S = zeros(1,lt);
for i = 1:lt
    S(i) = trapz(n1,integrand(:,i));
end
```

Bibliography

[1] T. H. Bell. Lee waves in stratified flows with simple harmonic time dependence. *J. Fluid Mech.*, 67:705–722, 1975.

[2] T. A. Coleman and K. R. Knupp. Factors affecting surface wind speeds in gravity waves and wake lows. *Wea. Forecasting*, 24:1664–1679, 2009.

[3] T. Dauxois and W. R. Young. Near-critical reflection of internal waves. *J. Fluid Mech.*, 390:271–295, 1999.

[4] C. Garret and E. Kunze. Internal tide generation in the deep ocean. *Annu. Rev. Fluid Mech.*, 39:57, 2007.

[5] C. Garrett. Mixing with latitude. *Nature*, 422:477–478, 2003.

[6] T. Gerkema and J. T. F. Zimmerman. *An introduction to internal waves. Lecture Notes.* URL `http://www.nioz.nl/nioz_nl/7336985ab4d76392af5eb51543bb253f.php`.

[7] I. S. Gradshteyn and I. M. Ryzhik. *Table of integrals, series, and products.* Elsevier (Singapore), seventh edition, 2007.

[8] C. H. Jiang and P. S. Marcus. Selection rules for the nonlinear interaction of internal gravity waves. *Phys. Rev. Lett.*, 102(124502), 2009.

[9] E. Kreyszig. *Advanced engineering mathematics.* John Wiley and Sons, Inc., eigth edition, 1999.

[10] P. K. Kundu, I. M. Cohen, and D. R. Dowling. *Fluid mechanics*. Academic Press, fifth edition, 2012.

[11] K. G. Lamb. Nonlinear interaction among internal wave beams generated by tidal flow over supercritical topography. *Geophys. Res. Lett.*, 46(L09313), 2004.

[12] J. Lighthill. Internal waves and related initial-value problems. *Dyn. Atmos. Oceans*, 23:3–17, 1996.

[13] M. J. Lighthill. *Waves in Fluids*. Cambridge University Press, 1978.

[14] D. E. Mowbray and B. S. Rarity. A theoretical and experimental investigation of the phase configuration of internal waves of small amplitude in a density stratified fluid. *J. Fluid Mech.*, 28:1–16, 1967.

[15] T. Peacock and A. Tabaei. Visualization of nonlinear effects in reflecting internal wave beams. *Phys. Fluids*, 17(061702), 2005.

[16] O. M. Phillips. *The Dynamics of the Upper Ocean*. Cambridge University Press, 1966.

[17] B. Sutherland. *Internal gravity waves*. Cambridge University Press, 2010.

[18] A. Tabaei and T. R. Akylas. Nonlinear internal gravity wave beams. *J. Fluid Mech.*, 482:141–161, 2003.

[19] A. Tabaei, T. R. Akylas, and K. G. Lamb. Nonlinear effects in reflecting and colliding internal wave beams. *J. Fluid Mech.*, 526:217–243, 2005.

[20] M. Tenenbaum and H. Pollard. *Ordinary differential equations*. Dover, 1985.

[21] S. A. Thorpe. On the reflection of a train of finite amplitude internal waves from a uniform slope. *J. Fluid Mech.*, 178:279–302, 1987.

[22] C. Wunsch and R. Ferrari. Vertical mixing, energy, and the general circulation of the ocean. *Annu. Rev. Fluid Mech.*, 36:281, 2004.